



## EVALUATION OF BORON NITRIDE NANOBARB AS THERMAL CONDUCTIVITY ENHANCERS TO CNT COMPOSITES

Title	EVALUATION OF BORON NITRIDE NANOBARB AS THERMAL CONDUCTIVITY ENHANCERS TO CNT COMPOSITES
Item Type	Thesis
Authors	Clark-Johnson, Lauren P.
URI	<a href="https://hdl.handle.net/10945/71051">https://hdl.handle.net/10945/71051</a>
Publisher	Monterey, CA; Naval Postgraduate School
Date Issued	2022-09
Rights	This publication is a work of the U.S. Government as defined in Title 17, United States Code, Section 101. Copyright protection is not available for this work in the United States.
Download date	2026-04-14 23:20:36
Link to Item	<a href="https://hdl.handle.net/10945/71051">https://hdl.handle.net/10945/71051</a>

Downloaded from NPS Archive: Calhoun



**NAVAL  
POSTGRADUATE  
SCHOOL**

**MONTEREY, CALIFORNIA**

**THESIS**

**EVALUATION OF BORON NITRIDE NANOBARB  
AS THERMAL CONDUCTIVITY ENHANCERS  
TO CNT COMPOSITES**

by

Lauren P. Clark-Johnson

September 2022

Thesis Advisor:  
Second Reader:

Claudia C. Luhrs  
Dragoslav Grbovic

**Approved for public release. Distribution is unlimited.**

THIS PAGE INTENTIONALLY LEFT BLANK

<b>REPORT DOCUMENTATION PAGE</b>			<i>Form Approved OMB No. 0704-0188</i>	
Public reporting burden for this collection of information is estimated to average 1 hour per response, including the time for reviewing instruction, searching existing data sources, gathering and maintaining the data needed, and completing and reviewing the collection of information. Send comments regarding this burden estimate or any other aspect of this collection of information, including suggestions for reducing this burden, to Washington headquarters Services, Directorate for Information Operations and Reports, 1215 Jefferson Davis Highway, Suite 1204, Arlington, VA 22202-4302, and to the Office of Management and Budget, Paperwork Reduction Project (0704-0188) Washington, DC, 20503.				
<b>1. AGENCY USE ONLY (Leave blank)</b>		<b>2. REPORT DATE</b> September 2022	<b>3. REPORT TYPE AND DATES COVERED</b> Master's thesis	
<b>4. TITLE AND SUBTITLE</b> EVALUATION OF BORON NITRIDE NANOBARB AS THERMAL CONDUCTIVITY ENHANCERS TO CNT COMPOSITES			<b>5. FUNDING NUMBERS</b>	
<b>6. AUTHOR(S)</b> Lauren P. Clark-Johnson				
<b>7. PERFORMING ORGANIZATION NAME(S) AND ADDRESS(ES)</b> Naval Postgraduate School Monterey, CA 93943-5000			<b>8. PERFORMING ORGANIZATION REPORT NUMBER</b>	
<b>9. SPONSORING / MONITORING AGENCY NAME(S) AND ADDRESS(ES)</b> N/A			<b>10. SPONSORING / MONITORING AGENCY REPORT NUMBER</b>	
<b>11. SUPPLEMENTARY NOTES</b> The views expressed in this thesis are those of the author and do not reflect the official policy or position of the Department of Defense or the U.S. Government.				
<b>12a. DISTRIBUTION / AVAILABILITY STATEMENT</b> Approved for public release. Distribution is unlimited.			<b>12b. DISTRIBUTION CODE</b> A	
<b>13. ABSTRACT (maximum 200 words)</b>  Boron nitride nanobarbs (BNNB) is a new material that is a powder version of Boron nitride nanotubes (BNNT). Studies have shown BNNT to be electrically insulating and thermally conductive. BNNT are difficult to incorporate in composite materials due to their tendencies to agglomerate. BNNBs have a shorter nanostructure, which makes them easier to incorporate in epoxy mixtures. This study examines the thermal conductive properties of BNNB in carbon nanotube (CNT) composites. In this study thermally conductive composites were created using various loadings of BNNB in a 0.5 weight percent CNT-Epoxy mixture. The specimens were tested for electrical conductivity and thermal conductivity using two methods. The electrical conductivity data collected concluded that at higher loadings of BNNB, the percolation limit could be reached. The thermal conductivity data from the forward looking infrared (FLIR) camera were inconclusive due to methodology issues; however, the results from the thermocouple data concluded that an increase in BNNB loading lead to an increase in thermal conductivity at a steady state temperature of 50C.				
<b>14. SUBJECT TERMS</b> boron nitride nanobarbs, BNNB, boron nitride nanotubes, BNNT, forward looking infrared, FLIR, carbon nanotube, CNT			<b>15. NUMBER OF PAGES</b> 81	
			<b>16. PRICE CODE</b>	
<b>17. SECURITY CLASSIFICATION OF REPORT</b> Unclassified	<b>18. SECURITY CLASSIFICATION OF THIS PAGE</b> Unclassified	<b>19. SECURITY CLASSIFICATION OF ABSTRACT</b> Unclassified	<b>20. LIMITATION OF ABSTRACT</b> UU	

THIS PAGE INTENTIONALLY LEFT BLANK

**Approved for public release. Distribution is unlimited.**

**EVALUATION OF BORON NITRIDE NANOBARB AS THERMAL  
CONDUCTIVITY ENHANCERS TO CNT COMPOSITES**

Lauren P. Clark-Johnson  
Lieutenant, United States Navy  
BA, Mount Holyoke College, 2013

Submitted in partial fulfillment of the  
requirements for the degree of

**MASTER OF SCIENCE IN MECHANICAL ENGINEERING**

from the

**NAVAL POSTGRADUATE SCHOOL  
September 2022**

Approved by: Claudia C. Luhrs  
Advisor

Dragoslav Grbovic  
Second Reader

Brian S. Bingham  
Chair, Department of Mechanical and Aerospace Engineering

THIS PAGE INTENTIONALLY LEFT BLANK

## **ABSTRACT**

Boron nitride nanobarbs (BNNB) is a new material that is a powder version of Boron nitride nanotubes (BNNT). Studies have shown BNNT to be electrically insulating and thermally conductive. BNNT are difficult to incorporate in composite materials due to their tendencies to agglomerate. BNNBs have a shorter nanostructure, which makes them easier to incorporate in epoxy mixtures. This study examines the thermal conductive properties of BNNB in carbon nanotube (CNT) composites. In this study thermally conductive composites were created using various loadings of BNNB in a 0.5 weight percent CNT-Epoxy mixture. The specimens were tested for electrical conductivity and thermal conductivity using two methods. The electrical conductivity data collected concluded that at higher loadings of BNNB, the percolation limit could be reached. The thermal conductivity data from the forward looking infrared (FLIR) camera were inconclusive due to methodology issues; however, the results from the thermocouple data concluded that an increase in BNNB loading lead to an increase in thermal conductivity at a steady state temperature of 50C.

THIS PAGE INTENTIONALLY LEFT BLANK

# TABLE OF CONTENTS

<b>I.</b>	<b>INTRODUCTION.....</b>	<b>1</b>
<b>A.</b>	<b>MOTIVATION .....</b>	<b>1</b>
<b>B.</b>	<b>BACKGROUND INFORMATION .....</b>	<b>1</b>
<b>1.</b>	<b>Carbon Nanotubes .....</b>	<b>2</b>
<b>2.</b>	<b>Boron Nitride Nanotubes .....</b>	<b>3</b>
<b>3.</b>	<b>Boron Nitride Nanobarbs.....</b>	<b>5</b>
<b>C.</b>	<b>RESEARCH OBJECTIVES .....</b>	<b>5</b>
<b>D.</b>	<b>THESIS OVERVIEW .....</b>	<b>5</b>
<b>II.</b>	<b>EXPERIMENTAL METHODS .....</b>	<b>7</b>
<b>A.</b>	<b>FABRICATION OF COMPOSITES.....</b>	<b>7</b>
<b>1.</b>	<b>Materials Used.....</b>	<b>7</b>
<b>2.</b>	<b>Dispersion Methods .....</b>	<b>9</b>
<b>3.</b>	<b>Curing Methods .....</b>	<b>11</b>
<b>4.</b>	<b>Sample Preparation and Polishing.....</b>	<b>11</b>
<b>B.</b>	<b>ELECTRICAL CONDUCTIVITY STUDY.....</b>	<b>12</b>
<b>C.</b>	<b>THERMAL CONDUCTIVITY STUDY .....</b>	<b>13</b>
<b>1.</b>	<b>Thermocouple with Thermal Grease .....</b>	<b>16</b>
<b>2.</b>	<b>Thermocouple with Thermal Tape.....</b>	<b>18</b>
<b>3.</b>	<b>FLIR.....</b>	<b>18</b>
<b>D.</b>	<b>CHARACTERIZATION .....</b>	<b>19</b>
<b>1.</b>	<b>Visual Inspection.....</b>	<b>19</b>
<b>2.</b>	<b>Optical Microscopy .....</b>	<b>19</b>
<b>3.</b>	<b>Scanning Electron Microscopy (SEM).....</b>	<b>21</b>
<b>4.</b>	<b>Energy Dispersive X-ray Spectroscopy (EDS) .....</b>	<b>21</b>
<b>III.</b>	<b>RESULTS AND ANALYSIS .....</b>	<b>23</b>
<b>A.</b>	<b>EXPERIMENTAL RESULTS.....</b>	<b>23</b>
<b>1.</b>	<b>Electrical Conductivity Data.....</b>	<b>23</b>
<b>2.</b>	<b>Thermal Conductivity Data .....</b>	<b>27</b>
<b>B.</b>	<b>PHYSICAL OBSERVATIONS .....</b>	<b>30</b>
<b>1.</b>	<b>Optical Microscope Analysis.....</b>	<b>31</b>
<b>2.</b>	<b>Porosity Size and Distribution .....</b>	<b>34</b>
<b>3.</b>	<b>SEM Imagery .....</b>	<b>40</b>
<b>4.</b>	<b>EDS Characterization.....</b>	<b>44</b>
<b>IV.</b>	<b>CONCLUSION .....</b>	<b>51</b>

<b>V.</b>	<b>DISCUSSION AND RECOMMENDATIONS.....</b>	<b>57</b>
<b>A.</b>	<b>FUTURE STUDIES.....</b>	<b>57</b>
<b>B.</b>	<b>PROCESS IMPROVEMENTS .....</b>	<b>58</b>
	<b>LIST OF REFERENCES.....</b>	<b>59</b>
	<b>INITIAL DISTRIBUTION LIST .....</b>	<b>63</b>

## LIST OF FIGURES

Figure 1.	Illustration of heat flows through a material. Source: [1].	2
Figure 2.	Carbon nanotube structure compared to other carbonations structures. Source: [4].	3
Figure 3.	Carbon nanotube structure (left) compared to Boron Nitride nanotube structure (right). Source: [8].	4
Figure 4.	LOCTITE EA9396. Source: [12].	8
Figure 5.	Left: TEM micrograph of boron nitride nanobarb at 40kX, Right: Bulk BNNB pulp provided by BNNano. Source: [9].	9
Figure 6.	FlackTek speed mixer	10
Figure 7.	Diagram of thermal conductivity experiment design.	14
Figure 8.	Arctic Silver 5 Thermal Grease. Source: [17].	16
Figure 9.	Nikon Epiphot 200. Source: [20].	20
Figure 10.	ZEISS Neon 40 field emission scanning electron microscope. Source: [21].	21
Figure 11.	Method 1: Electrical resistivity raw data of various BNNB loadings in 0.5 wt% CNT composites	24
Figure 12.	Method 2: Electrical resistivity raw data of various BNNB loadings in 0.5 wt% CNT composites	26
Figure 13.	Method 1 vs. Method 2 comparison of 5% BNNB 0.5% CNT loading electrical resistivity raw data	27
Figure 14.	Comparing methods of thermal conductivity measurements. Adapted from [18].	28
Figure 15.	FLIR data collection points.	30
Figure 16.	Various BNNB loadings in 0.5wt% CNT cured epoxy optical microscope image 2.5X	32
Figure 17.	Various loading of BNNB - 0.5 wt%C NT cured epoxy optical microscope images 10X.	33

Figure 18.	Optical microscope image of various BNNB loadings in 0.5% CNT composite used for imageJ analysis .....	35
Figure 19.	Pore area distribution of 0 wt% BNNB 0.5 wt% CNT .....	36
Figure 20.	Pore area distribution of 1 wt% BNNB 0.5 wt% CNT .....	37
Figure 21.	Pore area distribution of 3 wt% BNNB 0.5 wt% CNT .....	38
Figure 22.	Pore area distribution of 5 wt% BNNB 0.5 wt% CNT .....	39
Figure 23.	Pore area distribution of 10 wt% BNNB 0.5 wt% CNT .....	40
Figure 24.	Top: 1 wt% BNNB 0.5 wt% CNT SEM image 3000x, Bottom: 5 wt% BNNB 0.5 wt% CNT SEM image 3000x.....	42
Figure 25.	Top: 1 wt% BNNB 0.5 wt% CNT composite Bottom: 5 wt% BNNB 0.5 wt% CNT composite SEM image 10,000x.....	43
Figure 26.	5 wt% BNNB 0.5 wt% CNT SEM image 50,000x.....	44
Figure 27.	5 wt% BNNB 0.5 wt% CNT SEM image 3000x used for EDS characterization. spot 1 (RED), spot 2 (TEAL), spot 3 (ORANGE), spot 4 (YELLOW) .....	45
Figure 28.	5 wt% BNNB 0.5 wt% CNT EDS results spot 1 (top) and spot 2 (bottom).....	46
Figure 29.	5 wt% BNNB 0.5 wt% CNT EDS results spot 3 .....	48
Figure 30.	5 wt% BNNB 0.5 wt% CNT EDS results spot 4 .....	49
Figure 31.	Porosity of various BNNB loadings .....	51
Figure 32.	Resulting Thermal Conductivity data from thermal couple data collection design that has been normalized with area variation and porosity .....	53
Figure 33.	Top: 1% BNNB, Bottom 5% BNNB loading.....	55

## LIST OF TABLES

Table 1.	Dimensions of 1018 Steel and composites for Thermal Conductivity calculations. Adapted from [10]. .....	16
Table 2.	5 wt% BNNB 0.5 wt% CNT EDS quantitative results spot 1 (top) and spot 2 (bottom) .....	47
Table 3.	5 wt% BNNB 0.5 wt% CNT EDS quantitative results spot 3 .....	48
Table 4.	5 wt% BNNB 0.5 wt% CNT EDS quantitative results spot 4 .....	49
Table 5.	Thermal Conductivity error caused by composite cross-sectional area deviations .....	53

THIS PAGE INTENTIONALLY LEFT BLANK

## LIST OF ACRONYMS AND ABBREVIATIONS

ATSM	American Society for Testing and Materials
BSD	back-scatter detector
BN	boron nitride
BNNT	boron nitride nanotube
BNNB	boron nitride nanobarbs
CE	cyanate ester
CNT	carbon nanotube
CVD	chemical vapor deposition
CCVD	catalytic chemical vapor deposition
DOD	department of defense
EMI	electromagnetic interference
EDS	energy dispersive x-ray spectra
FLIR	forward-looking looking infrared
NA	not available
NIH	National Institute of Health
NPS	Naval Postgraduate School
OM	optical microscope
PCB	printed circuit board
PDF	powder diffraction file
RPM	rotations per minute
SEM	scanning electron microscopy

THIS PAGE INTENTIONALLY LEFT BLANK

## ACKNOWLEDGMENTS

I would like to thank the faculty and staff for their support throughout my time at Naval Postgraduate School. I would also like to thank my advisor Professor Claudia Luhrs for her support and encouragement while working on my thesis and the many classes I had under her instruction. Completing my graduate degree has always been a dream of mine. I am grateful for the U.S. Navy providing me with this opportunity. I would also like to thank my family for their love and support while I pursue my graduate degree, without which I would have not been able to be where I am today. Will, you have provided me with constant love and encouragement, you are an amazing partner, father, and friend. Beth, you came to help our family when it was most critical for me finishing my degree. Without you being with us all our efforts may have been lost. Walt, I get my strength every day from your toothless smile and bright glowing eyes.

THIS PAGE INTENTIONALLY LEFT BLANK

# I. INTRODUCTION

## A. MOTIVATION

The purpose of this study is to determine the thermal properties of carbon nanotube (CNT) composites, when using Boron Nitride Nanobarbs are dispersed. If proven to be thermally conductive, this technology can be use in interference shielding systems in satellite designs. This study will benefit the DOD due to the varying applications it can support. Specifically, the use of CNT/epoxy composite 3D printed objects have the potential to be useful in multiple aerospace applications.

Aerospace designs have looked to utilize the electrical properties of CNT due to their lightweight nature. We aim to improve the thermal conductivity of CNT epoxy composites with BN Nanobarbs additives. Aerospace resin has no electrical conductivity. We add CNT to enable electricity to flow through resin for printed electronic applications. With these additives, they are still not thermally conductive. Adding BN Nanobarbs should improve thermal conductivity. Boron Nitride Nanotubes have been successfully studied and shown to improve thermal conductivity when added to Carbon Nanotube epoxy composites. This is the first study examining the effects of Boron Nitride in the barb structure on those composites.

## B. BACKGROUND INFORMATION

Why is thermal conductivity important? Thermal conductivity is the rate at which heat is transferred through a material. The idea is shown in Figure 1. In remote environments it is desired to have a material that can remove heat generated by electronic circuitry efficiently to extend the lifetime of the device in such environment. In satellite design where space and weight are at a premium being able to incorporate thermal dissipation into the structural components of its electronics without the need of adding additional parts is paramount in good design. By enhancing our electrically conductive composites with thermally conductive additives we are developing a method to prevent the degradation of critical electrical components in the composite material made enclosures.

The goal is to achieve increased thermal conductivity with the addition of boron nitride nano barb.

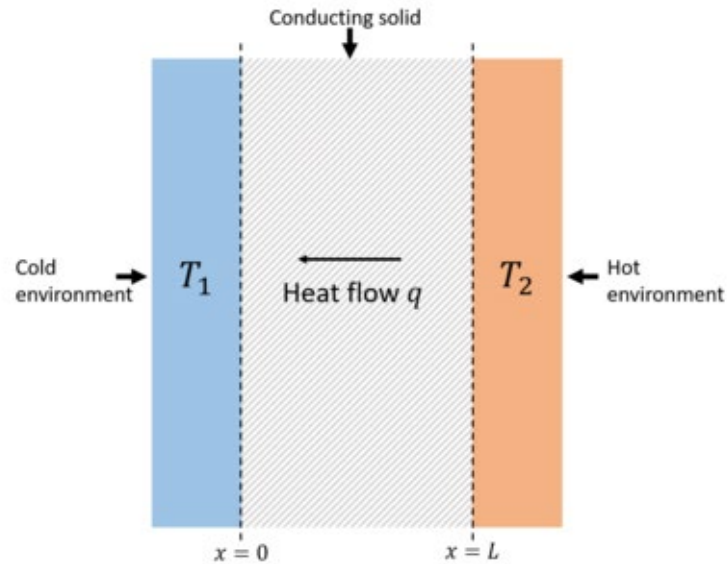


Figure 1. Illustration of heat flows through a material. Source: [1].

## 1. Carbon Nanotubes

Carbon Nanotubes provides the electrical conductivity in the composite. It has been heavily researched and has been lauded for its high tensile strength and low weight. The high tensile strength of CNT is due to its covalent  $sp^2$  bonds. CNT also benefits from its uniform packing structure which allows it to conduct electricity very efficiently [2]. Carbon nanotubes have been shown to allow for electrical transport at very low loadings such as 0.1wt% [3]. An example of CNT is shown in section H of Figure 2. Figure 2 also shows examples of other carbonaceous structures such as (A) diamond, (B) graphite, (C) Lonsdaleite, (D) C60 fullerene, (E) C540 fullerite and (G) amorphous carbon.

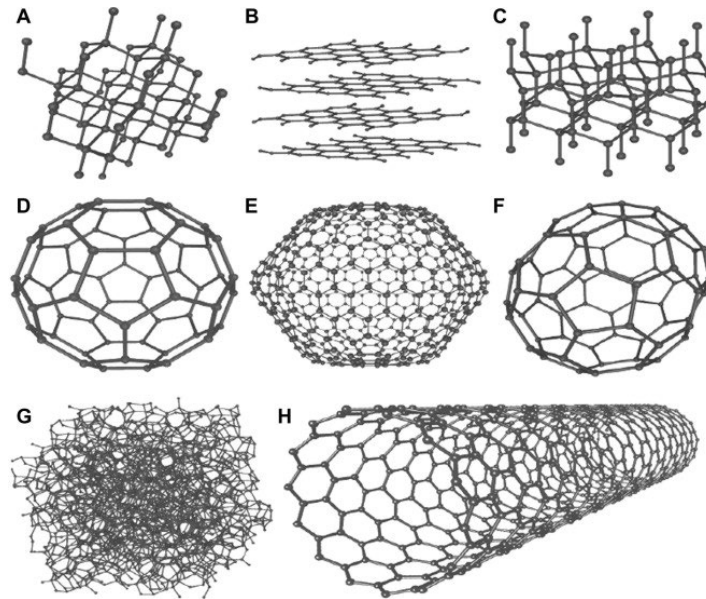


Figure 2. Carbon nanotube structure compared to other carbonations structures. Source: [4].

Chemical vapor deposition (CVD) with a metal catalyst is typically used in creating a large volume of CNT. CNTs have historically been used as conductive elements in plastics due to their high aspect ratio of being able to form percolation networks at very low weight percentages [5]. Percolation systems involving CNTs networks occur where there is an efficiently and tight paths of CNT systems in an insulating mass [6]. CNTs can form electrically conductive networks even at high aspect ratios of 0.1wt% CNTs to filler material [5]. CNTs have been used in this form in automotive industry for charge dissipation in fuel liners. Whereas in the microelectronics industry CNTs have been used for electromagnetic interference (EMI) shielding [5]. Whilst CNTs are great for charge dissipation, at low loadings their ability to exhibit significant thermal dissipation is limited. Thermal conductivity of CNTs is affected by its density, structural defects and temperature amongst other things [7].

## 2. Boron Nitride Nanotubes

Boron Nitride Nanotubes, BNNTs, have a similar size and structure to CNTs as shown in Figure 3. Both are both around 1 nm in diameter and are made up of rolled up hexagonal lattices. Unlike CNT which has carbon at every point in the lattice structure,

BNNT alternates boron and nitrogen at each lattice point. BNNT has in-plane lattice constants of 2.5 Å compared to CNT which has in-plane lattice constants of 2.46 Å. The lattice constant refers to the distance between the unit cells in a crystal structure which are directly proportional to the distance between atoms in the lattice. Since BNNT has Nitrogen, a larger atom, in the crystal lattice constant is larger. However, the interlayer stacking of BNNT is smaller than that of CNT due to the smaller boron atoms layering directly over the larger nitrogen atoms. [8]. The interlayer stacking of CNT allows it to perform like a semimetal whereas BNNT will perform as a semiconductor [8].

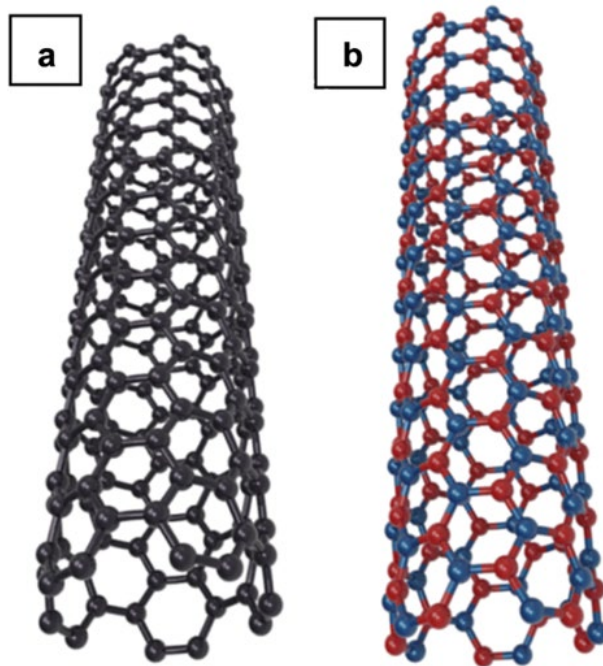


Figure 3. Carbon nanotube structure (left) compared to Boron Nitride nanotube structure (right). Source: [8].

BNNT has been claimed to outperform its carbonaceous elemental neighbor in numerous ways [9]. Thermal conductivity for BNNT is expected to be high due to the parent material h-BN having high thermal conductivity. BNNT can be synthesized in a catalytic chemical vapor deposition (CCVD) or using a ball milling technique. The result is a spun cotton ball like structure of BNNT [10].

### **3. Boron Nitride Nanobarbs**

Boron Nitride Nanobarbs (BNNB) improve upon BNNT in multiple of ways. BNNB reduces the Van der Waals attraction by minimizing the contact area between the particles. This enables the BNNB to be mixed into other materials with less agglomeration. The shorter barb like structures also helps its incorporation in composites. BNNB are electrically resistive, thermally conductive and strong. When compared to CNT BNNB are more stable at higher temperatures.

#### **C. RESEARCH OBJECTIVES**

The purpose of this research is to establish the feasibility of Boron Nitride Nanobarbs material to be used as a thermal conductivity enhancing layer for Carbon Nanotube Composites. It is believed that producing CNT composites with higher thermal conductivity will allow the materials to last longer and serve for a wider number of applications. Given that the CNT composite has acceptable levels of electrical shielding and charge dissipation we will examine how that property changes by the addition of non-electrically conductive BN.

Boron Nitride has good thermal conductivity. One of the things we are expected to see is the electrical conductivity to decrease and thermal conductivity to increase as we add BN to the aerospace resin nanotube composition. The result of this thesis should guide future studies of how to optimize the combination of BN Nanobarbs to the aerospace resin nanotube ratio so that we can achieve enhanced thermal conductivity while still maintaining electrical conductivity.

#### **D. THESIS OVERVIEW**

This study hypothesizes that adding Boron Nitride Nanobarbs will greatly increase the thermal conductivity of the composites produced. The addition of boron nitride alone will have the greatest impact of increasing thermal conductivity over fabrication methods. Other factors like porosity were not overlooked.

Chapter II presents details about the materials and fabrication processes used to produce thermally conductive composites as well as the equipment and methods used to

characterize and test those composites. In order to test the hypothesis required close attention to the precise steps in the protocol of preparing the CNT-BNNB loaded samples.

Chapter III introduces the results of the BNNB characterization as well as the results from the electrical conductivity and thermal conductivity measurements. This section seeks to explain and correlate the data with additional studies of the physical make-up of the BNNB samples.

Chapter IV discusses the implications of the results chapter and what future studies could be done to further this research.

Chapter V summarizes the critical findings of this thesis. Overall, we observed an increase in thermal conductivity when increased loadings of BNNB were added to the CNT-epoxy composites.

## II. EXPERIMENTAL METHODS

As previously mentioned, the goal of this study was to increase the thermal conductivity of epoxy composites. In this chapter, the three variations of how to obtain an epoxy resin-carbon nanotube (CNT)-boron nitride nanobarbs (BNNB) composites are described, as well as the characterization techniques employed to identify the microstructural features of the samples. After an appropriate weight ratio of the three components (epoxy-CNT-BNNB) was achieved using an asymmetric mixer, the samples were cured, and electrical conductivities were measured. Following the electrical conductivity measurements, the thermal conductivity was measured using two methods: an infrared thermal camera (FLIR) and using thermocouples.

### A. FABRICATION OF COMPOSITES

In creating the epoxy-resin-CNT-BNNB mixture, the goal was to achieve even consistency, and homogeneous dispersion of carbon nanotubes as well as boron nitride nanobarbs while having minimal air pockets in the epoxy resin curing process. The three variations of the composite synthesis employed different dispersion and curing methods. The fabrication route for the composite material had three stages. The first stage was the dispersion of the BNNB. The second was the dispersion of the CNTs. The third was the curing of the epoxy resin mixture. Following the synthesis of each method was a visual inspection of the composite samples. Only one of the mixing and curing strategies was used in the electrical and thermal conductivity study.

#### 1. Materials Used

This section describes the Carbon Nanotube Pulp, the Boron Nitride Pulps and polymeric resin used to create the composite samples.

##### *a. Epoxy Resin*

For this study, the epoxy used was Aero EA 9396 LOCTITE (Henkel Corporation, Dusseldorf, Germany). This is a two-part epoxy which is typically used to bond substrates together. The two parts, are designated part A and part B. Part A, is green to dark purple in

color. Part A contains epoxide and bis-phenol compounds while part B contains polyfunctional amine hardeners [11]. After combining part A with part B, the epoxy was cured at either room temperature over a period of 3 to 5 days or in a furnace heated to 66 °C over an hour. The two-part epoxy mixes at a 100:30 ratio by weight with a work time of 75 to 90 minutes after hardener is added. The product is featured in Figure 4.



Figure 4. LOCTITE EA9396. Source: [12].

***b. Carbon Nanotube Pulp***

Huntsman Corporation supplied the CNT pulp used for this study. The CNT is manufactured from a chemical vapor deposition method using methane and an iron catalyst. As a result, from the CVD process carbon sheets and hydrogen are produced. The CNT pulp is milled from the carbon sheets produced using chemical vapor deposition (CVD). Huntsman Corporation approximate the pulp size to be 0.05 mm in diameter by 1 mm in length [13]. High electrical conductivity has been found with low loadings of 1 weight percent or less [14]. Throughout this study a CNT loading of 0.5 wt% was used.

*c. Boron Nitride Nanobarb Pulp*

BNNano provided the BNNB pulp for this study and owns the process of developing a powder, barb-like version of Boron Nano Tubes. This product has a similar atomic structure as described in the BNNT section with a hexagonal packing structure with alternating boron and nitrogen at each lattice point. However, its bulk material form is a grey-white powder as shown in Figure 5. This study used BNNB from BNNano batch 200107. The working hypothesis of this thesis is that BNNB could be an effective additive in composites to improve their thermal conductivity in the same fashion that other boron nitride products. The company describes the BNNB pulp to appear rock candy-like in structure giving way to its “nano barb” terminology [9]. The powder’s applicability to this research is due to its short barb-like structures and being a powder will tend to agglomerate less than the other commercial products and easier to mix and disperse in the epoxy matrix employed. BNNano accomplishes this by reducing the Van der Waals Attraction in their design of BNNBs. This study examines how the barb-like structure of the boron nitride affects electrical conductivity and its effects on the thermal conductivity of the CNT-epoxy resin composites.

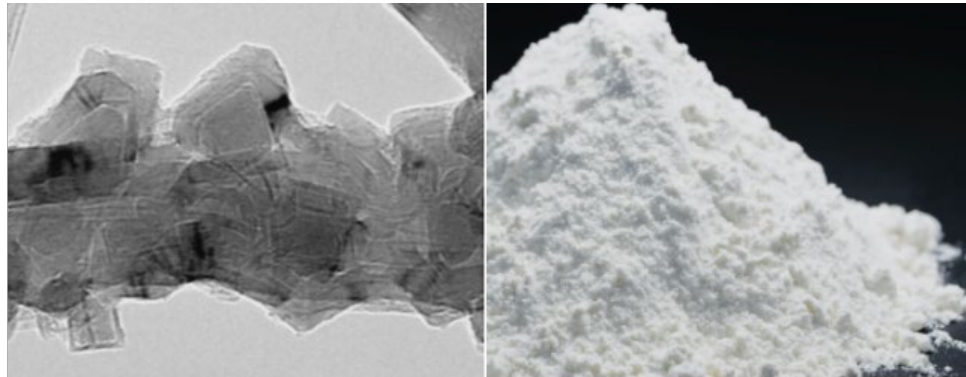


Figure 5. Left: TEM micrograph of boron nitride nanobarb at 40kX, Right: Bulk BNNB pulp provided by BNNano. Source: [9].

**2. Dispersion Methods**

Two methods of dispersion were used. The first method combined the CNT Pulp with the BNNB Pulp. Only method one was used for 0 wt% and 3 wt% BNNB in 0.5 wt%

CNT-epoxy. The second method is to mix the BNNB pulp first, then mix in the CNT pulp. The second method used 1 wt%, 3 wt%, 5 wt% and 10 wt% loadings of BNNB in 0.5 wt% CNT-epoxy. The pulps were mixed with a FlackTek asymmetric mixer as shown in Figure 6. The BNNT loading percentages were selected to study the effects of BNNT on electrical conductivity and thermal conductivity. The weight percentage for CNT was selected to be 0.5 wt% from historical studies demonstrating a highly electrically conductive sample [14].



Figure 6. FlackTek speed mixer

The steps for the first method are outlined below:

Weigh BNNB and CNT for desired loadings and add to part A (epoxy resin), mix in asymmetric mixer in 4 cycles increasing progressively the mixing speed from 1200 to 2500 and 3000 rpm. In between mixing cycles submerge the lower part of the plastic cup containing the sample in a water bath to reduce the temperature while applying vacuum

using a roughing pump to remove air from the mixture. The 4 cycles were conducted using intervals of 2, 1, 1 and 3 minutes respectively. Add part B and mix at 3000 rpm for 1 min.

The steps for the second method are similar to the first, however, the BNNB were first completely mixed into part A, using the 4 cycles described above, followed then by the addition of the CNT, with 4 extra cycles of mixing, cooling and applying vacuum.

### **3. Curing Methods**

BNNB-CNT composites were cured in a binder oven at 66°C for one-hour in accordance with LOCTITE manufacturer instructions in an air atmosphere [11]. While curing in the furnace, the composite pucks were also placed in a vacuum chamber to reduce porosity. The effects of porosity were examined later in this study.

The third method that was used follows the same steps as above however during the curing process the samples were placed in a glass container that was piped to a roughing pump so that the samples will cure under a low-grade vacuum. The third method used 1 wt%, 3 wt%, 5 wt% and 10 wt% loadings of BNNB. The resulting samples were used in the follow-on electrical conductivity and thermal conductivity studies.

### **4. Sample Preparation and Polishing**

Following the synthesis of the samples were prepared the thermal conductivity experiments. First two steel blocks were cut to into a rectangular prism at the desired dimensions 15 x 15 x 20 mm. Next the composite samples were cut to 5 x 15 x 15mm using a precision wet cut off machine. The composites were hand polished on a Buehler Ecomet 4 polisher using P300, P500, P800, P1200 then P1500 grit paper at 5, 10, 15, 20 minute intervals.

To make the insulation housing, insulation was cut to fit around three sides of the experimental set up. A small 15mm by 15mm lid for the experimental set up was cut and placed on top of the set up.

## B. ELECTRICAL CONDUCTIVITY STUDY

To conduct the electrical conductivity study, a four-point printed circuit board was employed. The Printed Circuit Board or PCB is a “four-point collinear probe which uses a method that involves bringing four equally spaced probes in contact with a material of an unknown resistance” [15]. The PCB allows for 8 measuring points so an average and error can be calculated. To prepare the PCBs for the study, they are first cleaned to remove any debris from the surface, and two rows of tape are placed along the tape guidelines. The CNT-BNNB epoxy is deposited on the surface and distributed using a glass microslide to ensure an even layer is applied to the surface of the PCB. After the PCB covered with epoxy is set in binder oven to cure at 66°C for one-hour as described in the section above. After curing the tape is removed.

To find the electrical conductivity of our samples we took the inverse of the resistivity measured. For these purposes of this report only the resistivity was reported.  $\sigma$  is conductivity;  $\rho$  is resistivity.

$$\text{Equation 1. } \sigma = 1/\rho.$$

Resistivity is the electrical resistance per cross-sectional area of a conductive material. Resistivity has the dimensions of ohms meter. However, for thin films, like in this case, the standard units are ohm cm. Factors such as the electronic structure and temperature can affect the resistivity of a material. Since the addition of Boron Nitride Nanobarbs has a different electrical makeup from carbon nanotubes, it is important to observe how greatly the dilution of the epoxy impacts its overall electrical conductivity. From Ohm’s Law, we can deduce resistance, R. V is voltage and I is current.

$$\text{Equation 2. } R = V/I.$$

Resistivity,  $\rho$ , was derived from the known dimensions of the specimen using Pouillet’s Law. Where A is the cross-sectional area of the material, L is the length or thickness of the material and R is the electrical resistance. Since our measuring sample was

1 cm x 1 cm square, both its length and width were equal (L). Also, cross sectional area was  $A = L t$ . Therefore, we could write the expression for conductivity the following way:

$$\text{Equation 3. } \rho = RA/L = Rt.$$

In order to measure the resistivity of our samples various currents were ran through the outer electrodes using a Keithley power source. Various currents were assigned; 5, 10, 20, 50, 100, 150, 200, 300, 400, and 500  $\mu$ Amps. The resulting voltage drop was measured using a digital multimeter and recorded onto a spreadsheet. The process was repeated for all 8 locations on the circuit board.

### C. THERMAL CONDUCTIVITY STUDY

Thermal conductivity describes how well heat is transferred from one object to another. In examining the thermal conductivity two methods were employed, the use of a forward looking infrared thermal camera (FLIR) and thermocouples. The FLIR method used a directed to the surface perpendicular to the direction of heat flow and the use of thermocouples placed at each surface boundary. The experiment and insulation housing design remained the same between the two methods for repeatability. Figure 7 shows the locations where measurements were taken for the thermal conductivity study. In order to find the temperature change across the 1018 steel block we took a measurement at the hotplate (T1) and another at the top of the steel block (T2). To measure the temperature change across the composite we took measurements below the composite as it was heated by the steel block (T2) and at above the composite (T3). When the top of the second steel block had reached steady state, no longer changing temperature (T4) the experiment concluded.

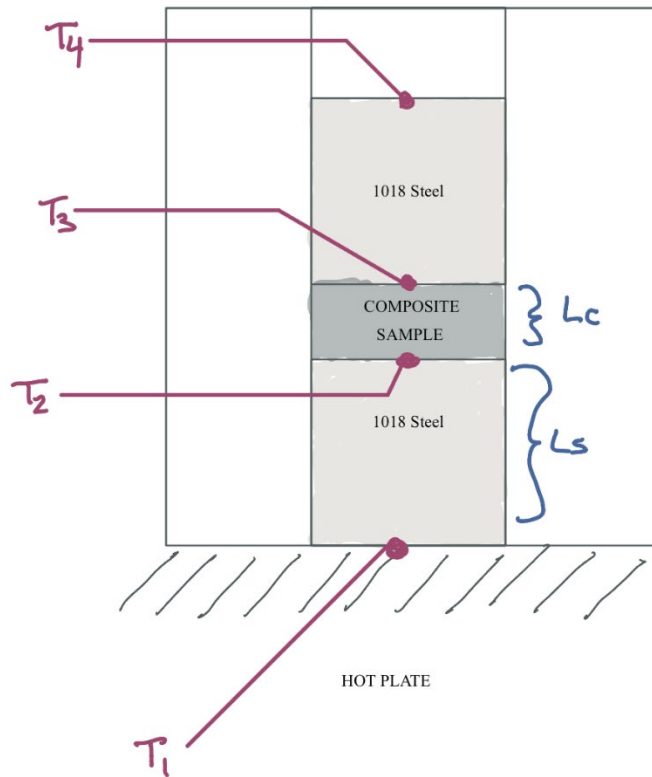


Figure 7. Diagram of thermal conductivity experiment design

In previous studies the samples were fully enclosed to prevent any thermal gains from the sides. This design had an exposed wall for the FLIR camera to be able to take measurements along the side of the stack.

This study made several key assumptions. One being the contact surface area of the steel perfectly matched the contact surface area of the composite so that the interfacial resistance was negligible. To accomplish the near negligible interfacial thermal resistivity, thermal tape and thermal grease were used to improve surface contact. The use of thermal grease proved to be difficult in achieving experiment repeatability since the amount of thermal grease used lead to inconsistencies of the contact area between the steel and composite. It was also assumed that the thermal spreading resistance from surface area differences between the steel and the composite could also be neglected, thus  $A_s = A_c$ .

Conduction resistance refers to the internal resistance where heat dissipates into the environment [16]. Another assumption was that the conduction resistance that could result from one wall of the experimental set up being exposed to the air was negligible. The final assumption was that the temperature of the hotplate, steel and composite had reached a steady state and was no longer heating. In these assumptions, perfect heat transfer between the steel and composite was achieved, thus  $Q_s = Q_c$ . By being able to set  $Q_s = Q_c$  Equations 5 and 6 could be also set to equal each other to then solve for the composite's thermal conductivity.

$$\text{Equation 4. } K = Q \times L / A \times \Delta T,$$

We can rewrite Equation 4 in terms of heat transfer,  $Q$ , for both heat transfer of the composite and of the steel,

$$\text{Equation 5. } Q_s = [K_s \times A_s \times (T_2 - T_1)] / L_s,$$

$$\text{Equation 6. } Q_c = K_c \times A_c \times (T_2 - T_3) / L_c$$

Assuming perfect heat transfer  $Q_c = Q_s$ , Equation 5 is set to equal Equation 6,

$$\text{Equation 7. } K_s \times A_s \times (T_2 - T_1) / L_s = K_c \times A_c \times (T_2 - T_3) / L_c.$$

Now the term for the thermal conductivity  $K_c$  of the composite is isolated,

$$\text{Equation 8. } K_c = K_s \times A_s \times L_c \times (T_2 - T_1) / A_c \times L_s \times (T_2 - T_3),$$

Assuming that the contact area of the steel block is the same as the contact area of the composite,  $A_s$  can cancel out  $A_c$  to reduce Equation 8 to,

$$\text{Equation 9. } K_c = K_s \times L_c (T_2 - T_1) / (T_2 - T_3) \times L_s.$$

$K_s$  is the thermal conductivity of 1018 steel and was found on Matweb.  $L_c$  is the thickness of the composite sample and  $L_s$  is the thickness of the lower steel block, both

were found using calipers.  $T_1$  is the temperature of the hotplate.  $T_2$  is the temperature at the top of the lower steel block.  $T_3$  is the temperature at the top of the composite and  $T_4$  is the temperature at the top of the second steel block.

If everything is correct,  $K$  should be much smaller than  $K_s$ . If the addition of BNNB improves thermal conductivity of the CNT composite, then  $K_c$  will be larger than the  $K_{CNT}$  composite.

Table 1. Dimensions of 1018 Steel and composites for Thermal Conductivity calculations. Adapted from [10].

Parameters	Specifications
1018 Steel Thermal Conductivity, $K_s$	51.9
1018 Steel Block Thickness (mm.)	19.9
0 BN WT % Composite Thickness (mm.)	5.09
1 BN WT % Composite Thickness (mm.)	5.0
3 BN WT % Composite Thickness (mm.)	5.28
5 BN WT % Composite Thickness (mm.)	4.7
10 BN WT % Composite Thickness (mm.)	4.57

### 1. Thermocouple with Thermal Grease



Figure 8. Arctic Silver 5 Thermal Grease. Source: [17].

In the first attempt of measuring thermal conductivity using thermal couples' thermal grease was used as an interface material. Interface materials enhance the thermal contact between two surfaces to reduce their interfacial resistance [16]. Thermal grease is designed to have great heat transfer. While the thermal resistivity is proprietary to the manufacturer it is assumed to be very low or negligible.

First, the thermal couples were prepared for the thermal conductivity experiment setup. An Omega RDXL6SD Six Channel Handheld Temperature Data Logger was used in conjunction with four thermocouple leads to measure thermal conductivity of the composite sample. The leads were attached from the read-out component to the appropriate locations in the experiment set up. Next, the hot plate was set to 50 degrees Celsius. The thermal couple assigned to the hot plate was adhered to using Arctic Silver 5 thermal paste. It was important to apply the paste to the entire top and bottom surface of the 1018 steel block. A second thermal couple was then placed on top of the 1018 steel block. The thermal housing was placed around the block while the temperature approached a steady state at the second thermal couple. After a steady state for the lower steel block is reached, Arctic Silver 5 thermal paste is applied to cover the entire surface of the top and bottom of the composite sample, and the composite is placed on the lower steel block so that the edges are flush. The third thermal couple is placed on top of the composite. A second 1018 steel block, with thermal paste on the top and bottom surface, is placed on top of the composite with a fourth thermal couple adhered to its top. Thermal housing is replaced to surround the entire experimental setup. The read-out is set to record mode. When all the thermal couples reach a steady state, the record mode is turned off, and the experiment ends. The data is collected and using Equation 8 the thermal conductivity is calculated.

This method did not achieve reliable results because the amount of thermal grease used provided us with a wide variation in the thermal contact area between materials. Due to the concern of the thermal paste degradation causing gradual overheating and uneven coverage limitations this method was abandoned.

## **2. Thermocouple with Thermal Tape**

Since there was concern over the repeatability of using thermal grease in the thermal couple experiment design, the design was altered to use thermal tape as an interface material instead. Thermal tape 3M THERM PAD ½-5-8815 was used. Using the same cut and polished composite samples and 1018 steel blocks as before, a layer of thermal tape was cut and adhered to cover the entire upper and lower surface of the 1018 steel blocks as well as the composite samples. Thermal tape is also applied to the hotplate at the location where the experiment will occur. Not all hot plates heat evenly so it was important to collect the data for this study where the heating element heat is most uniform. This was found using a FLIR camera and marked with a sharpie for repeatability.

After the thermal tape is applied the second layer of adhesive barrier is removed and the first thermal couple is placed to measure the heating of the hotplate. Next the second layer of the thermal tape adhesive barrier is removed from the first 1018 steel block. The block is placed on the thermal couple. The second thermal couple is placed on top of the 1018 steel block to measure its heating. The hot plate is turned on and set to 50 degrees Celsius. The thermal housing is placed around the steel block until steady state is achieved. Next the thermal housing is briefly removed to add the composite and secondary steel block. Like before the thermal tape adhesive barrier is removed on the upper and lower portions of the composite and the composite is placed on top of the lower 1018 steel block ensuring the edges are flush. A third thermal couple is adhered to the top of the composite via the thermal tape layer. The second 1018 steel block is placed on top of the composite with a final thermal couple placed on top of it. The thermal housing is placed around the experimental set up and the measurements commence. The experiment concludes when the fourth thermal couple observes a steady state has been reached [18]. Data is extracted and analyzed.

## **3. FLIR**

FLIR method mirrored the set-up of the Thermocouple method. Each layer used thermal tape as the interface material as described above. A FLIR ETS320 camera was set up to face perpendicular to the exposed observational plane of experimental stack at a 7cm

working distance using mounting brackets. After the lower steel block had reached a steady state temperature of 50°C the composite and second steel block with the interface material was added. The exposed observational plane of the experimental stack was covered in electrical black tape as recommended by the FLIR manufacturer instructions to increase emissivity and have a uniform reflective surface to measure from [19]. Data collection points were selected in the FLIR tools program to best represent the plane where heat is transferred from steel to composite and from composite to steel. When the temperature had reached a steady state thermal conductivity was calculated.

#### **D. CHARACTERIZATION**

The structural analysis of the CNT-BNNB composites was conducted using visual inspection, optical microscopy, scanning electron microscopy (SEM), and Energy Dispersive X-ray Spectroscopy (EDS) as described in the next sections.

##### **1. Visual Inspection**

After each epoxy synthesis of the BNNB-CNT composites a visual inspection of the surface features was conducted. This was used as a qualitative tool to determine the effectiveness of curing process and observation of porosity.

##### **2. Optical Microscopy**

Nikon Epiphot 200 collected optical microscopy images at 2.5x and 10x magnification. Optical Microscope images captured the porosity of the various BNNB weight percentage loadings.

To prepare each sample for microscopy imaging, the pucks were cut using the precision wet cut off machine as used before, then mounted in a clear epoxy puck using Struers Epofix resin and hardener and set to cure for 24 hours. After the curing had completed the samples were placed in the Buehler Ecomet 4 polisher using a jig matching the dimensions of the pucks. Care was taken to ensure the pucks were distributed even and flat to the polishing surface. The pucks were polished using P1000 grit polishing paper at 15 N of pressure for 15 minutes. Followed by polished using P1500 grit polishing paper at 15 N of pressure for 20 minutes. Then by polished using P2500 grit polishing paper at 15

N of pressure for 25 minutes. Then by polished using P4000 grit polishing paper at 15 N of pressure for 30 minutes. Water was used as a lubricant throughout this process. In between each step the jig was removed, and the samples were flushed with deionized water to remove any residual silica from the polishing paper. Finally, the samples were polished using Buehler polishing cloth at 10 N of pressure for 5 minutes. Alumina and water were used as lubricant at this phase. Following the polishing the samples were placed in a Branson ultrasonicator facing downward with a mix of ethanol and water for 20 seconds then blown dry using compressed air.

During the optical microscope imaging, for each loading sample 5 images were taken at various locations throughout the sample, so that an average porosity could be found. ImageJ was used to compare pore amounts and size in the various BN loadings. ImageJ is an open-source measurement tool provided by NIH that uses pixel counts that, for this research, was used to measure porosity sizes.



Figure 9. Nikon Epiphot 200. Source: [20].

The images captured while using the Nikon Epiphot 200 optical microscope were then analyzed to ascertain the average porosity of each BNNB loading.

### 3. Scanning Electron Microscopy (SEM)

ZEISS Neon 40 field emission scanning electron microscope was used to capture SEM images. An example of the ZEISS Neon 40 can be seen in Figure 10. Images were collected using the InLens detector with an accelerating voltage of 20 kV, an aperture size of 30 $\mu$ m and a working distance of 5mm. Images were taken at 3 kx, and 10 kx. The CNT-BNNB composites were mounted in a clear Struers Epofix epoxy puck that was finely polished. The polishing enabled a smooth mirror like surface so that SEM could capture images of the microstructure of the composite samples. By fine tuning the contrast the CNT network could be distinguished in the composite sample. The goal of the SEM images was to capture the locations of the Boron Nitride Nanobarbs and Carbon Nanotubes. ImageJ was used to generate a depth map of the SEM images.



Figure 10. ZEISS Neon 40 field emission scanning electron microscope.  
Source: [21].

### 4. Energy Dispersive X-ray Spectroscopy (EDS)

Energy Dispersive X-ray Spectroscopy in the ZEISS Neon 40 was used to identify the elemental components of the SEM image. EHT was set to 20kV with a working distance of 5 mm. All images were collected with InLen beam. The samples observed were of polished 1 and 5 weight percent loadings of BNNB in 0.5 weight percent CNT- cured epoxy pucks. This tool helped verify the locations of the Boron Nitride.

THIS PAGE INTENTIONALLY LEFT BLANK

### III. RESULTS AND ANALYSIS

#### A. EXPERIMENTAL RESULTS

This section discusses results from the experimental portion. The first portion discusses results from the electrical conductivity experiment. This experiment evaluated the effects of various BNNB loading on the resistivity of the 0.5 wt% CNT/epoxy composite sample. It also evaluated the effect of the way in which the composite was made on conductivity. Next, we compare the results from the thermal conductivity data. In this section we see the results from various BNNB loadings on thermal conductivity measures using two methods, FLIR and thermocouples.

##### 1. Electrical Conductivity Data

In the electrical conductivity experiment we sought to understand the effects the addition of boron nitride nanobarbs had on a known electrically conductive carbon nanotube composite. While boron nitride is thermally conductive it is considered poorly electrically conductive compared to carbon nanotubes. As we add more boron nitride to our cured epoxy mixture the resistivity of the material is to increase. This is due to conductivity being created when there exists a connected path of conductive material in a nonconductive media [22]. The resistivity of 0, 1, 3, 5 and 10 wt% BNNB 0.5 wt% CNT loadings in epoxy polymer using both synthesis methods can be seen in Figures 11–13. These loadings were chosen as to span low, middle and high loadings to potentially determine the percolation limit if it exists in these weight percentages. The percolation limit refers to the ability of the conductive material, here being CNT, to form a network sufficient to conduct a charge [3]. The increased loadings of BNNB lead to the decrease in density of CNT networks. Increasing the loading of BNNB lead to increased resistivity, or less conductivity. This is due to a less robust three-dimensional CNT network [22]. As more BNNB is added to the composite the more of a buffer will exist in-between CNT network sites, thus less robust networks of CNT per area to move a charge.

As we see in Figure 11, using Method 1 the resistivity increased as more BNNB was added. The 1, 3, 5 wt% BNNB 0.5 wt% CNT loadings references Method 1's epoxy

synthesis where both CNT and BNNB are combined at the same time and mixed into the epoxy. When increasing from 0% BNNB to 1% BNNB the resistivity increased by a factor of 3.04. When increasing the loading of BNNB from 1% to 3% the resistivity increased by a factor of 1.38. Interestingly, when increasing BNNB loading from 3% to 5% there was a negligible factor of increased resistivity.

The standard deviation varied the greatest at this loading. The standard deviation for method 1 5wt% BNNB loading ranged from 47.6 to 46.6 ohms cm or 24.2 – 23.7% of the resistivity. The standard deviation for 3 wt% BNNB loading ranged from 30 to 29.5 ohms cm or 14.9 – 15.2% of the resistivity. The standard deviation for 1wt% BNNB loading ranged from 26.4 to 27.6 ohms cm or 18.2 – 19.2% of the resistivity. The standard deviation for 0 wt% BNNB loading ranged from 3.82 to 5.23 ohms cm or 8.3 – 11.1% of the resistivity.

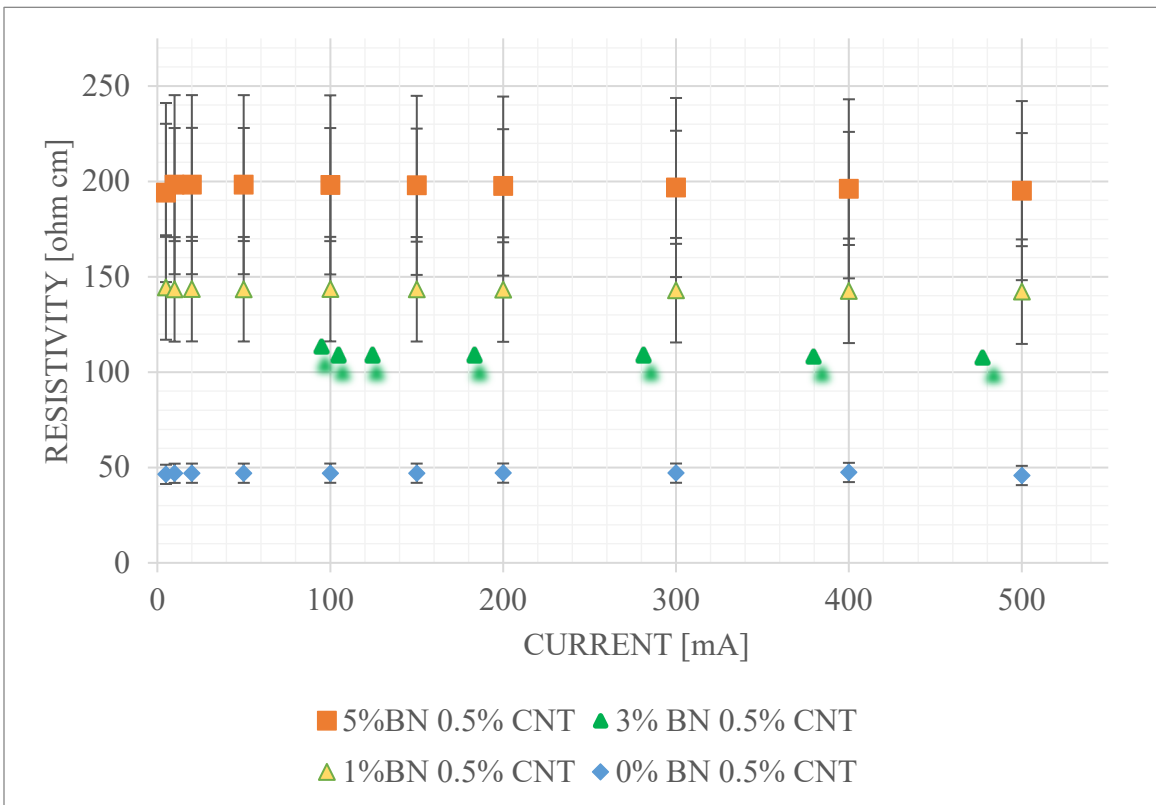


Figure 11. Method 1: Electrical resistivity raw data of various BNNB loadings in 0.5 wt% CNT composites

Similarly, as in Method 1, in Method 2, shown in Figure 12, the resistivity increased as more BNNB was added. Method 2 references where the BNNB is mixed in prior to the CNT for better incorporation. When increasing from 0% BNNB to 1% BNNB the resistivity increased by a factor of 1.72. Compared to Method 1, the resistivity improves by a factor of 1.76. When increasing the loading of BNNB from 1% to 3% there was no appreciable increase to resistivity. When comparing the 3% loading of Method 2 to Method 1, the latter improves by a factor of 1.76. When increasing BNNB loading from 3% to 5% the resistivity increased by a factor of 4. The 10wt% BNNB was the only measurement that led to a decrease in resistivity as applied current increased. A possible explanation for this is that a percolation limit for the BNNB loading being reached. This would mean that there are no complete conductive paths through composites and increased current increases the possibility of tunneling. This was discussed in [22]. This may be due to the idea that the BNNB agglomerates around the CNT structures at this loading. The agglomeration of BNNB would inhibit CNT network formation. The agglomeration is discussed further on in the coming paragraphs.

The standard deviation for 10wt% BNNB loading ranged from 95.18 to 151.4 ohms cm or 9.2 – 19.1% of the resistivity. The standard deviation of the 10wt% BNNB loading resistivity data increased as applied current increased. The standard deviation varied the greatest at this loading. The standard deviation for 5wt% BNNB loading ranged from 41.65 to 43.40 ohms cm or 12.7 – 13.1% of the resistivity. The standard deviation for 3wt% BNNB loading ranged from 11.49 to 14.48 ohms cm or 14.5 – 17.2% of the resistivity. The standard deviation for 1wt% BNNB loading ranged from 7.32 to 7.80 ohms cm or 8.9 – 9.6% of the resistivity. The standard deviation for 0wt% BNNB loading ranged from 3.82 to 5.23 ohms cm or 8.3 – 11.1% of the resistivity. As the data shows as the loading of BNNB increases the greater the standard deviation for the resistivity occurs. When normalized against the resistivity the error remains in the same range throughout.

The higher BNNB loadings saw the greatest reduction in standard deviation of resistivity when using method 2. This is due to the more consistent incorporation of the BNNB with CNT in the epoxy using this method.

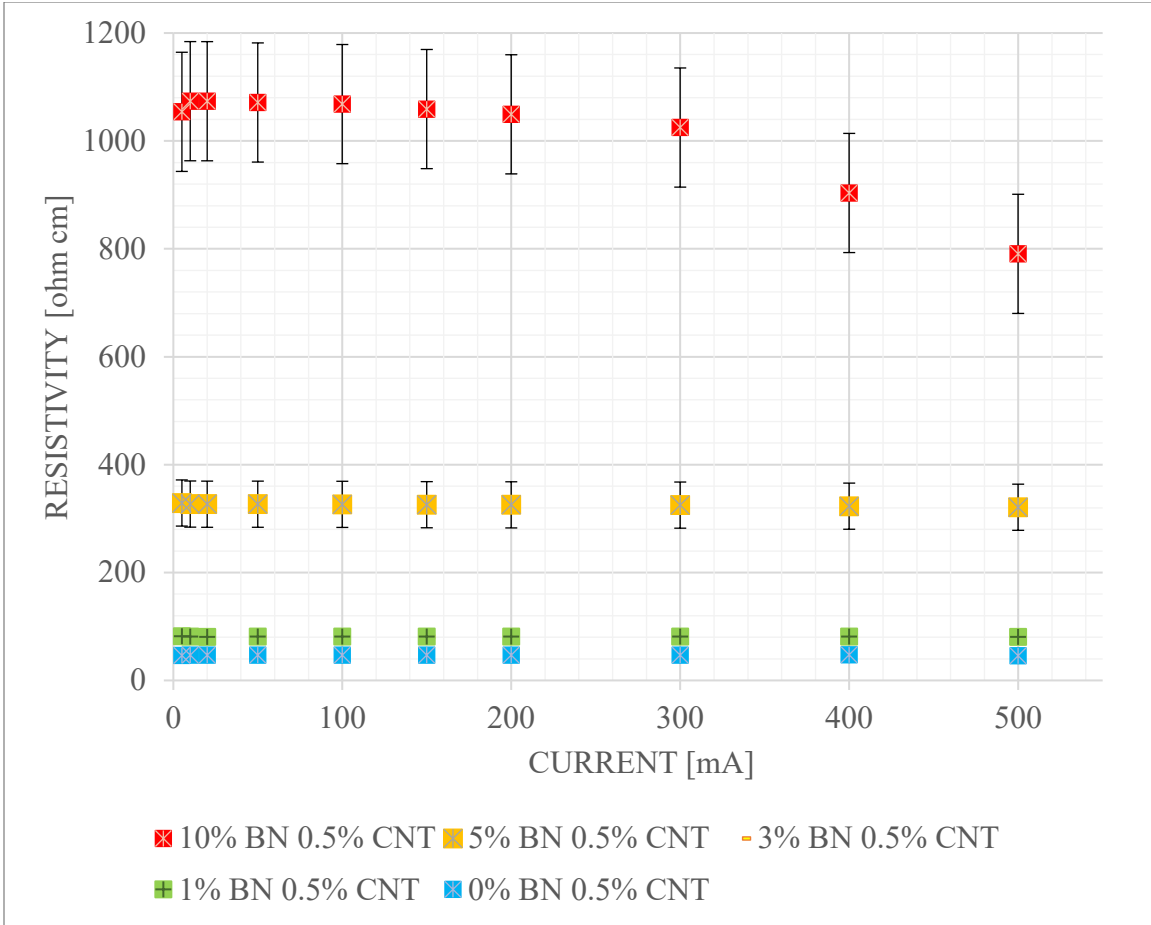


Figure 12. Method 2: Electrical resistivity raw data of various BNNB loadings in 0.5 wt% CNT composites

The Figure 13 illustrates how Method 2's 5 wt% BNNB loading benefited greatly with having lower resistivity than the unstaggered Method 1. This reduction in resistivity using Method 2 is also seen in 1, and 3 wt% BNNB sample as previously discussed. Here 5 wt% loading shows an improvement of a factor of 1.65. By staggering the incorporation of BNNB and CNT into the epoxy the mixture had less air in the mixture thus a lower resistance. Air pockets create areas of high resistivity since it greatly resists the flow of electric current.

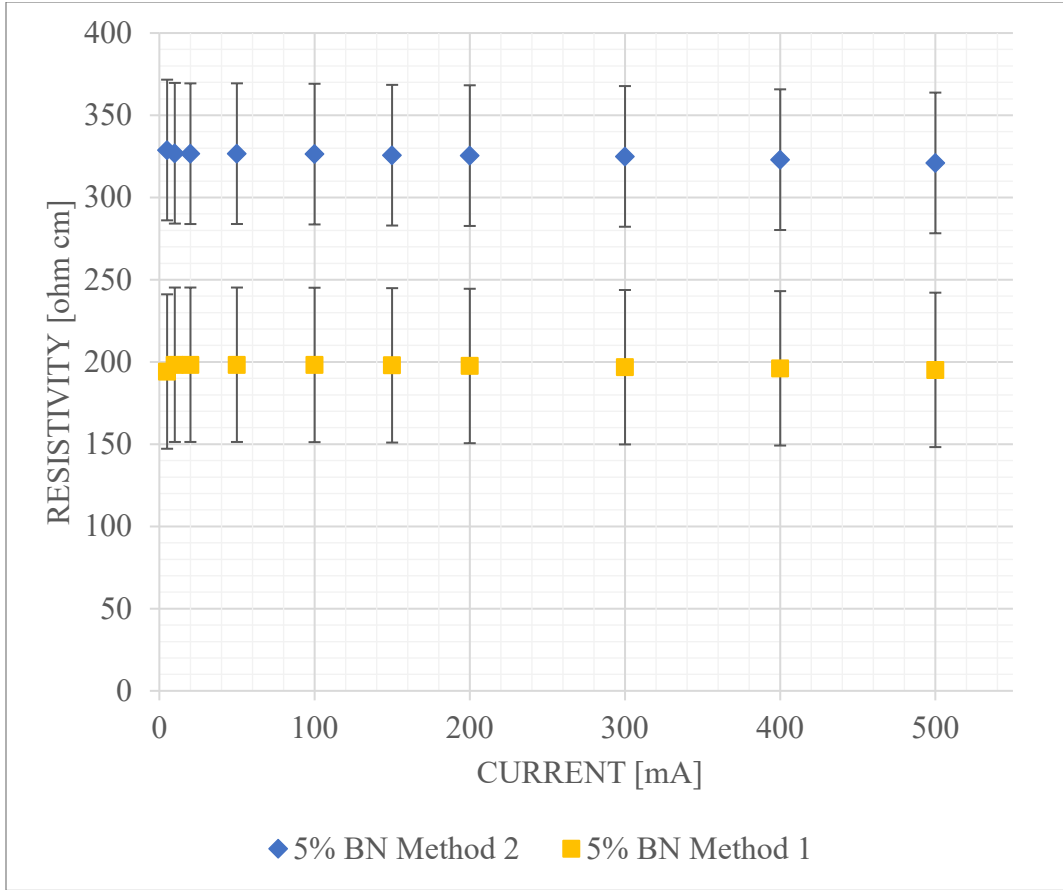


Figure 13. Method 1 vs. Method 2 comparison of 5% BNNB 0.5% CNT loading electrical resistivity raw data

## 2. Thermal Conductivity Data

In the thermal conductivity experiments we used a modified ASTM E1225 Longitudinal Heat Flow technique in order to find the thermal conductivity of our 0.5 wt% CNT composites at various BNNB loadings [18]. Figure 14. compares the resulting thermal conductivity gathered from the FLIR and Thermocouple experiments. Thermal conductivity of pure aero EA9396 epoxy is 0.20962 W/mK [23]. Thermal conductivity of 1018 steel is 51.9 W/mK. Steel is a great thermal conductor, so it makes sense that it has a much higher thermal conductivity value compared to the epoxy which is a poor thermal conductor. In these measurements it is observed that the thermal conductivity of 0.5 wt% CNT in epoxy is 1.83 (when measured via thermal couples) and 1.62 W/mK (when measured via FLIR). While it makes sense that there is a slight improvement when adding

CNT to the epoxy that it will have a higher value than from literature the range of data may not exactly match. Since the data was collected under identical conditions, it can be said that the trends of the data stand.

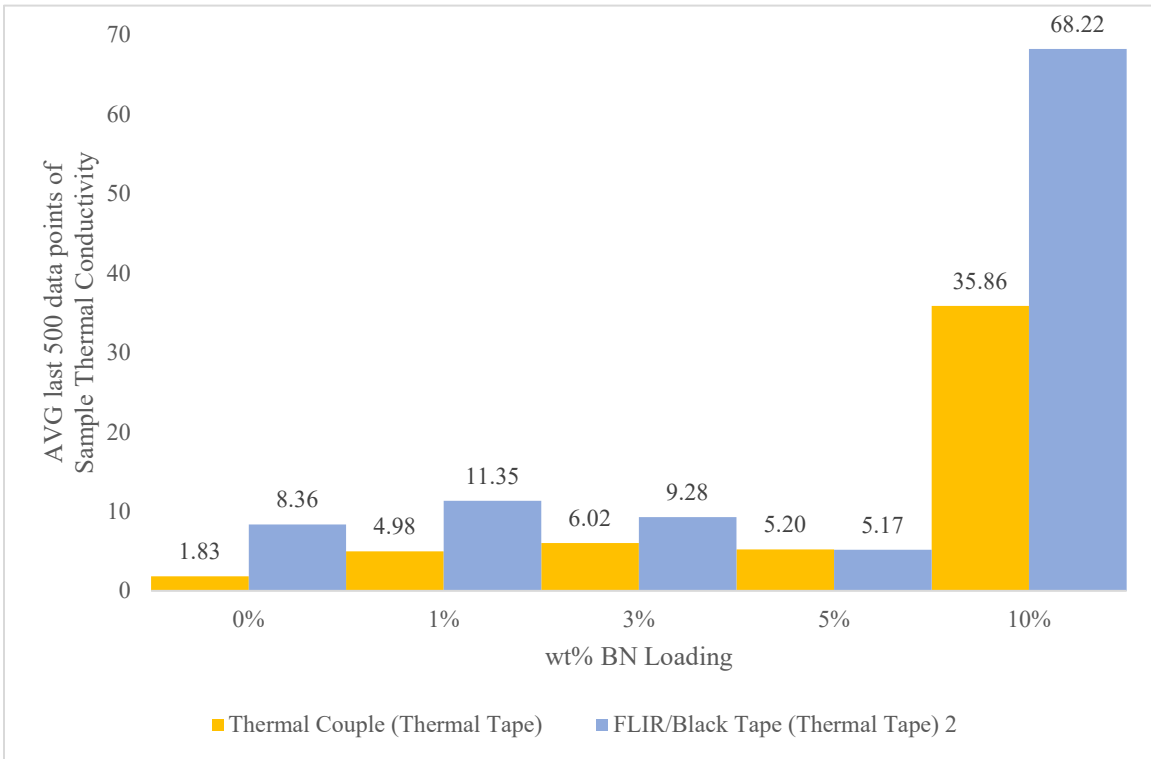


Figure 14. Comparing methods of thermal conductivity measurements. Adapted from [18].

From the thermocouple data we see that when increasing the loading of BNNB from 0 wt% to 1 wt% there is an increase in thermal conductivity by a factor of 272%. When the loading of the BNNB is increased to 3 wt% the thermal conductivity is increased by a factor of 328% from its baseline. In the thermocouple data's thermal conductivity trendline does not continue up at the 5 wt% loading, however it is still higher than its baseline by a factor of 284%. There were two observed flaws in the 5 wt% BNNB loading measurements. First was the drift in the hot plate temperature of 2.745 degrees. The second being the frame / minute rate was lower than in other experiments. The frame rate was 12 frames per minute versus the normal 60 frames per minute. The BNNB 10% saw the

greatest increase from the baseline by a factor of 196. From this data, is it reasonable to conclude that adding boron nitride nanobarbs will improve the thermal conductivity of CNT epoxy composites.

The FLIR data proved to be more challenging to decipher. When normalized to the baseline of 0.5 wt% CNT in epoxy the 1% loading increased thermal conductivity by a factor of 136%. This again happened for the BNNB 3 wt% loading where the thermal conductivity increased by a factor of 111%. However, when BNNB 5 wt% was measured it showed an decrease in thermal conductivity by a factor of 40% against the 0%BNNB 0.5% CNT baseline. In this experiment the observed thermal conductivity of the 10% BNNB loading had an increase by a factor of 816%. One source of error that occurred during the 3 wt% BNNB FLIR experiment was that the hotplate gradually dropped 5 degrees Celsius during the experiment, so steady state cannot be assumed in that reading. During the 5 wt% BNNB loading FLIR experiment the hotplate fluctuated 2.745 degrees Celsius so steady state cannot be assumed in this case either. Another flaw was discovered after reanalyzing the experiment setup. This was regarding possible shifts in the exact location where the FLIR gathered the thermal data during data collection. The arm that held the camera was not particularly robust and could have sagged slightly under the load of supporting the FLIR camera. If the focal point was not pinned exactly on the boundary in between the hotplate and the steel or in between the steel and the composite the recorded temperature will not reflect the temperature at the required location as demonstrated in Figure 7. Figure 15 shows the data collection point for all the FLIR measurements.

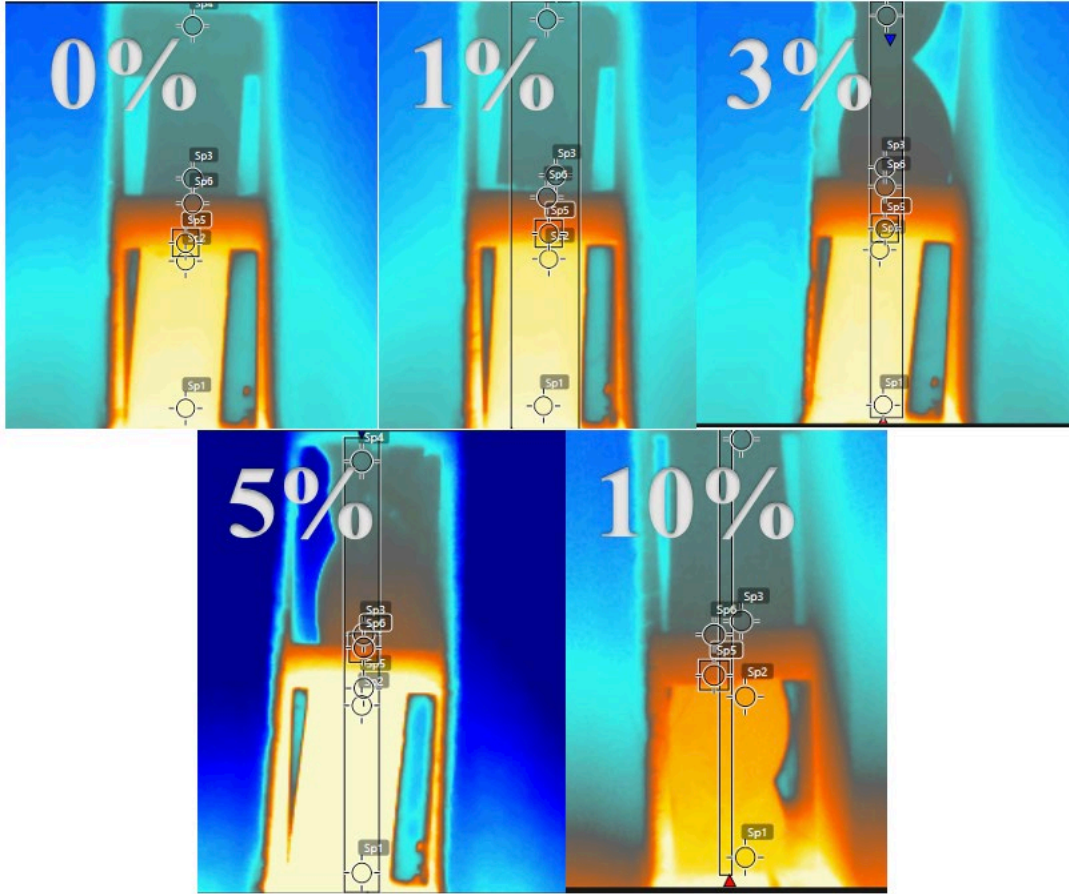


Figure 15. FLIR data collection points

The focal point of the FLIR takes an average of the nearest nine pixels to the location selected at the crosshairs of the image. These pixels even if the cross hairs are situated perfectly on the boundary between the hotplate and the steel or steel and the composite will record part of the temperature on the surface of each and average them together. While the FLIR data is not as reliable due to the reasons listed above, and excluding the 3 and 5 wt% BNNB, loading data points the data does show that the thermal conductivity increases by adding BNNB in the 0.5 wt% CNT composite.

## B. PHYSICAL OBSERVATIONS

In this section we examine how the structural properties of various loadings could explain the results found in the thermal conductivity studies as well as the electrical conductivity as discussed in the sections above. This section review images gathered and

analyzed using optical microscopy as well as scanning electron microscopy. The optical microscopy images were further analyzed using ImageJ to gather pore distribution histograms to better understand how porosity could affect thermal conductivity. Finally, we observe the distribution of BNNB using EDS data gathered in the SEM.

## **1. Optical Microscope Analysis**

Images 16–18 presents optical microscopy images of various loadings of BNNB-CNT composites. These images are from cured bulk samples of the composites used in the Thermal Conductivity study. These samples were cured in silicone pucks that ranged in 2–3 cm in thickness then cut using a diamond saw and polished as previously discussed in the methods section. Initially, it was a good idea to put a thicker layer of epoxy in the silicon mold to cure so that there will be enough material to observe in the thermal conductivity testing. The high presence of pores is what was observed via the optical microscope.

### ***a. 2.5X Images***

The optical microscope images of the BNNB at the magnification of 2.5X provides a broad image of the porosity distribution to be analyzed the upcoming sections. The images produced shows the porosity of the various loadings of BNNB in 0.5 wt% CNT in cured epoxy puck as well as other surface features.

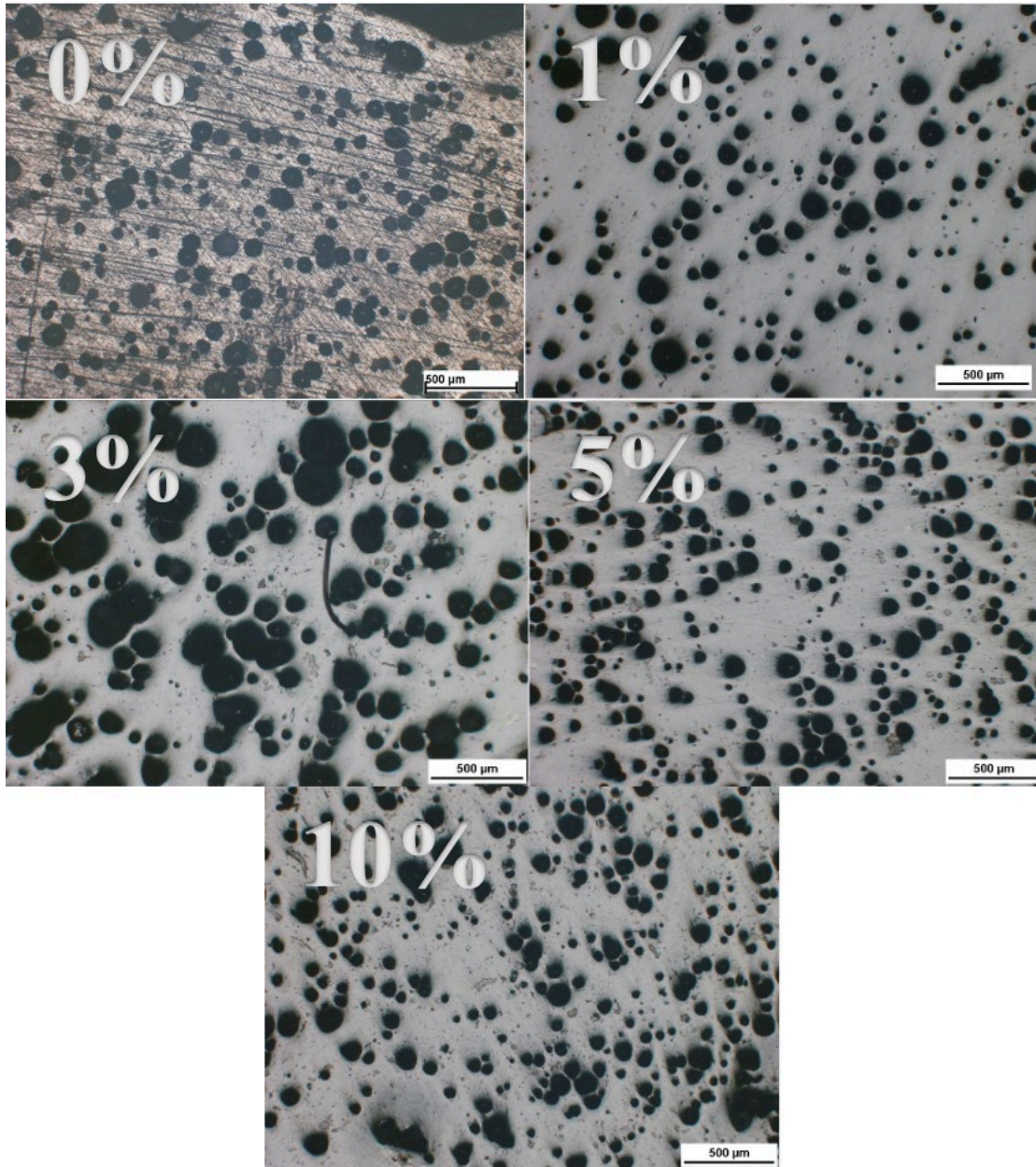


Figure 16. Various BNNB loadings in 0.5wt% CNT cured epoxy optical microscope image 2.5X

The images above show an anomaly in the size in the 3 wt% BNNB loading when compared to the other BNNB loading samples. The pores in the 3 wt% are unusually larger. The porosity was analyzed by ImageJ and an average pore size was found. When 3 wt% loading is compared to 5 wt% loading the average pores size are larger by a factor of  $3.91\mu\text{m}^2$ . This may be due to a methodology error in curing the 3 wt% BNNB 0.5 wt%

CNT epoxy sample. The average pore size of 0wt% BNNB loading is  $788.7 \mu\text{m}^2$ . The average pore size of 1 wt% BNNB loading is  $4404.9 \mu\text{m}^2$ . The average pore size of 3wt% BNNB loading is  $11,623.6 \mu\text{m}^2$ . The average pore size of 5 wt% BNNB loading is  $2,968.3 \mu\text{m}^2$ . The average pore size of 10 wt% BNNB loading is  $710.7 \mu\text{m}^2$ .

***b. 10X Images***

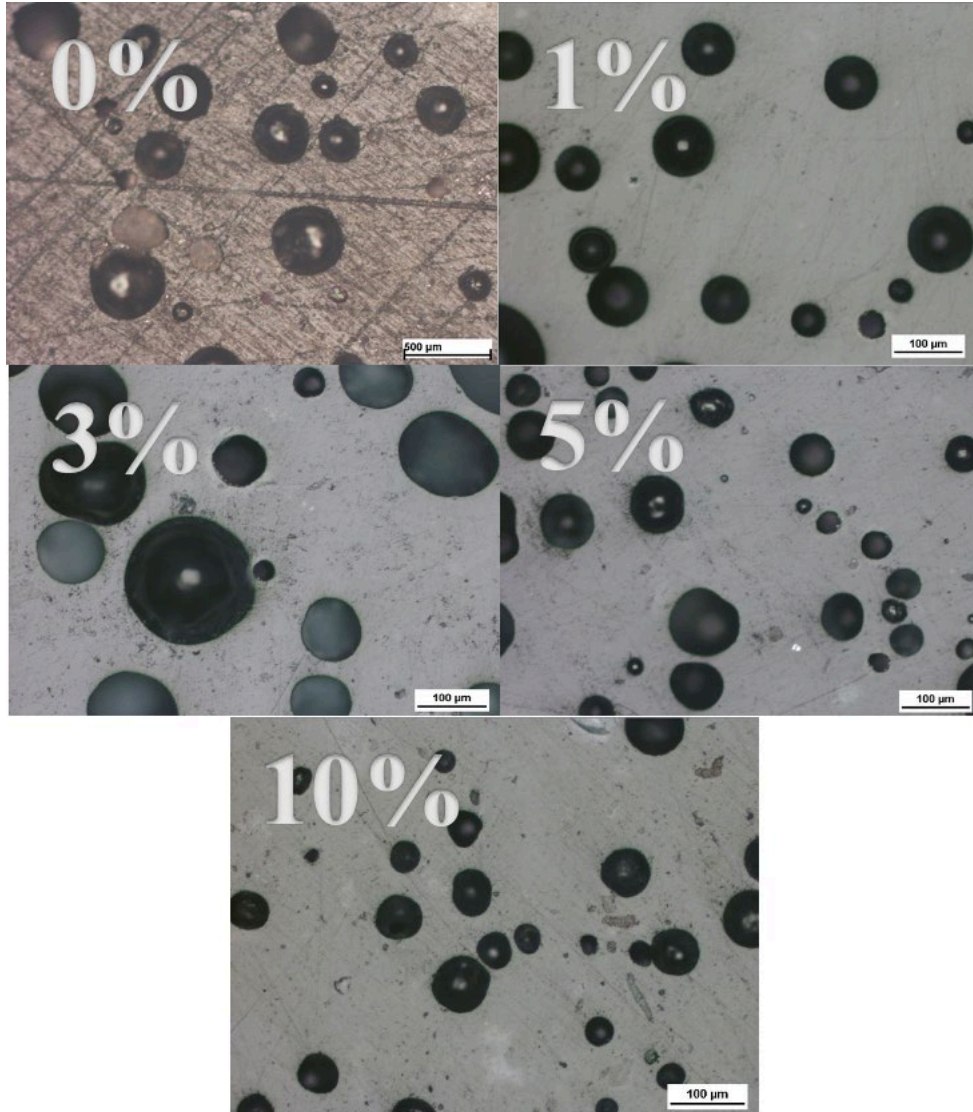


Figure 17. Various loading of BNNB - 0.5 wt% CNT cured epoxy optical microscope images 10X

The 10x optical microscope images show a closer morphology of the pores.

## **2. Porosity Size and Distribution**

This section discusses what sizes and amount of surface pores were found in the various BNNB loadings of cured epoxy samples. When considering Figure 18, visual observation shows that pores from the 3 wt% BNNB loading has significantly larger pores. The pores found at the 5 wt% BNNB are much smaller, more evenly dispersed and in the same relative size. The 1wt% had the least number of pores compared to the other loadings. It is important not to conflate the loading effects with what could be a result of uneven resin curing in a volume. Factors like low grade thermal run away may be at fault for causing the additional porosity. Thermal run away occurs when a puck of epoxy is cured too quickly, or the thickness of the mass exceeded is curing limitations. Thermal run away was not considered when creating the pucks used for the thermal conductivity experiments. These pucks were made from the remaining resin mixture after the four-point boards were created. The mixture was then deposited into a greased silicon mold. In thermal run away the chemical reaction between the epoxy and hardener generates too much causing the mixture to become hot and frothy [24]. In more extreme uncontrolled cures, the process the heat generated can be so excessive that it could melt a plastic container holding the mixture. The pucks when cured had a grew in size and porous structure. The best parts of these samples were cut to size and prepared as previously discussed.

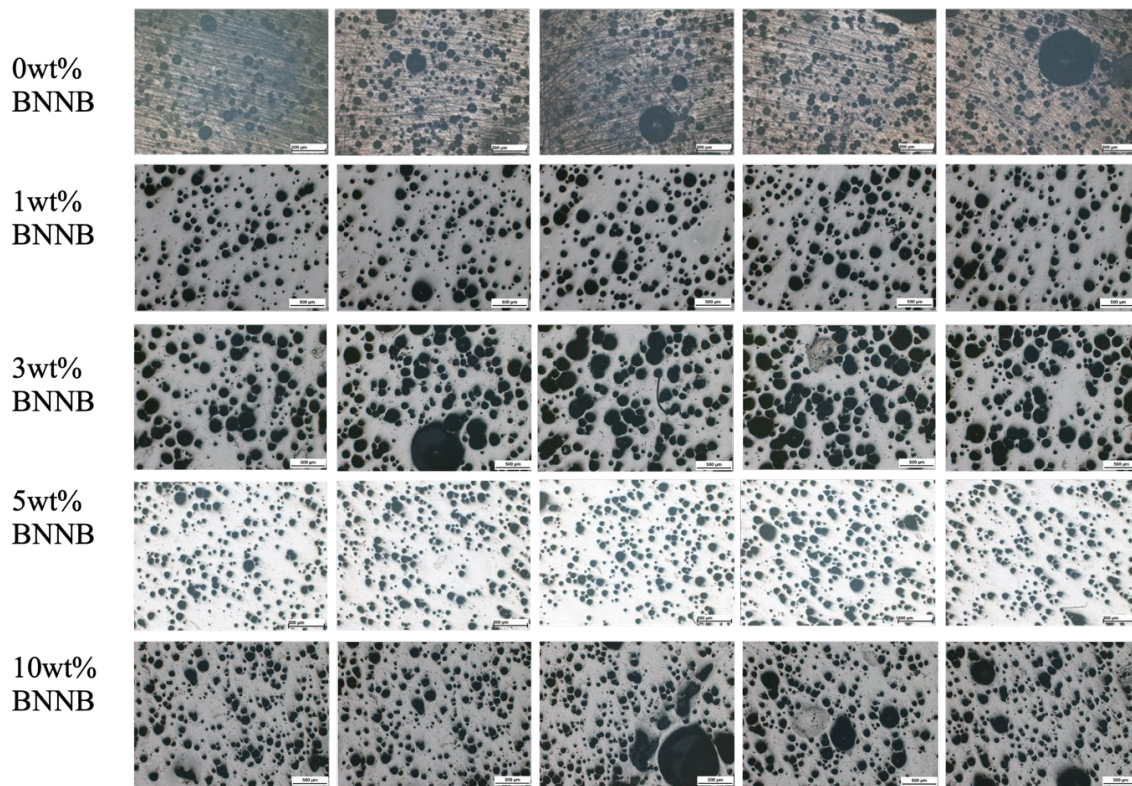


Figure 18. Optical microscope image of various BNNB loadings in 0.5% CNT composite used for imageJ analysis

To calculate the pore size in the cured pucks the images above were analyzed in imageJ to find the porosity size distribution for each BNNB loading composite sample. A mask was used to isolate the pores on the program and the particles were analyzed to collect the area they took up in the image. The total porosity was then compared to the total observed area to find the percent porosity of the image. Five locations of the sample were compared to find the average porosity percentage and standard deviation of the porosity sizes. The pore size distributions are shown in Figure 19.

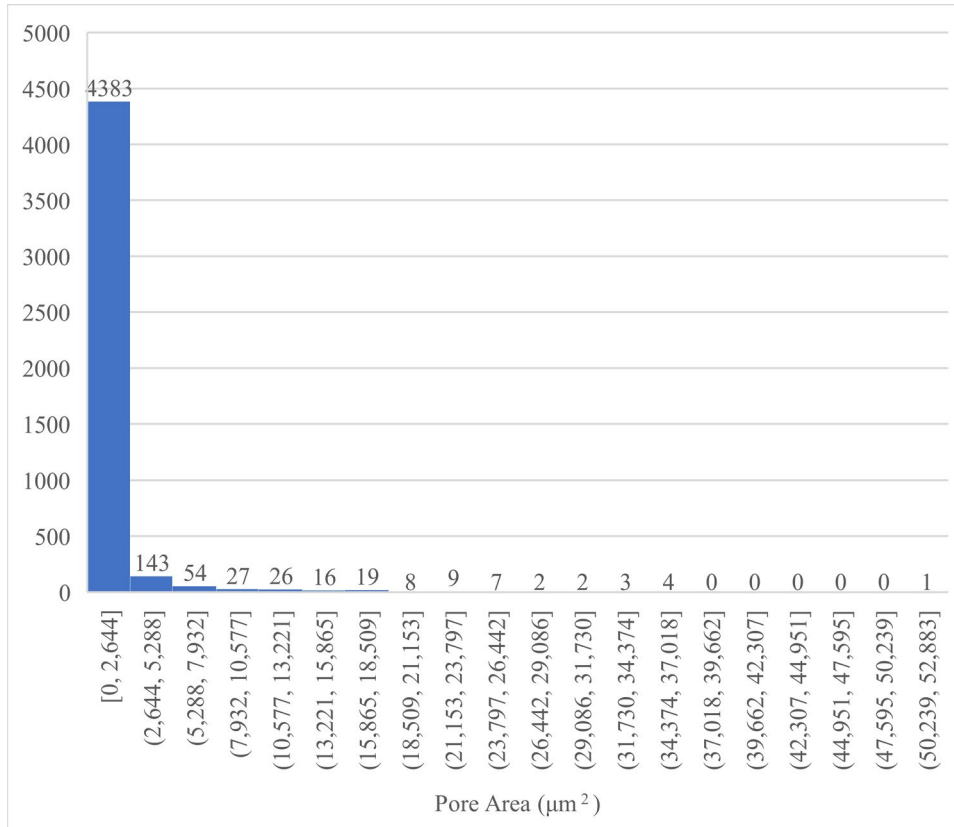


Figure 19. Pore area distribution of 0 wt% BNNB 0.5 wt% CNT

Over an observational area of 21,501,492 square micrometers there was 4704 pores observed in the 0 wt% BNNB sample. 93% of the porosity distribution occurring in the 0–2,644  $\mu\text{m}^2$  range. 3% of the porosity distribution occurring in the 2,644–5,288  $\mu\text{m}^2$  range. The increase of porosity drops in occurrence the larger the pore becomes. In the five sampled areas across the 0 wt% BNNB loading puck the percentage of the surface covered in pores ranged from 8.5% to 23%. The average surface area porosity percentage was 17.03%. The standard deviation of the porosity area was 3,034.8  $\mu\text{m}^2$ .

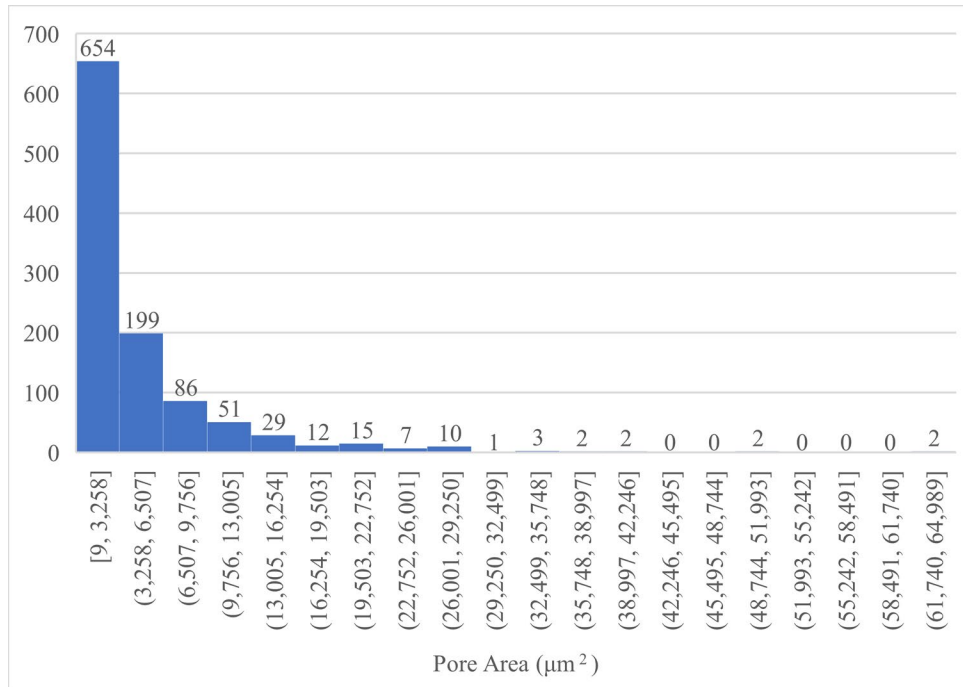


Figure 20. Pore area distribution of 1 wt% BNNB 0.5 wt% CNT

In the 1 wt% BNNB sample an area of 27,506,568  $\mu\text{m}^2$  was observed. In that area there was 881 pores. The pores 74% of the porosity distribution occurring in the 0–3,258  $\mu\text{m}^2$  range. 22% of the porosity distribution occurring in the 3,258 – 6,507  $\mu\text{m}^2$  range. 9.8% of the porosity distribution occurring in the 6,507 – 9,756  $\mu\text{m}^2$  range. From this data it can be deduced that most of the pores were larger than that of the 0 wt% BNNB sample however fewer pores were present. Similarly, the increase of porosity drops in occurrence the larger the pore becomes. In the five sampled areas across the 1wt% BNNB loading puck the percentage of the surface covered in pores ranged from 13.12% to 22.44%. The average surface area porosity percentage was 17.23%. The standard deviation of the porosity area was 6,711.71  $\mu\text{m}^2$ .

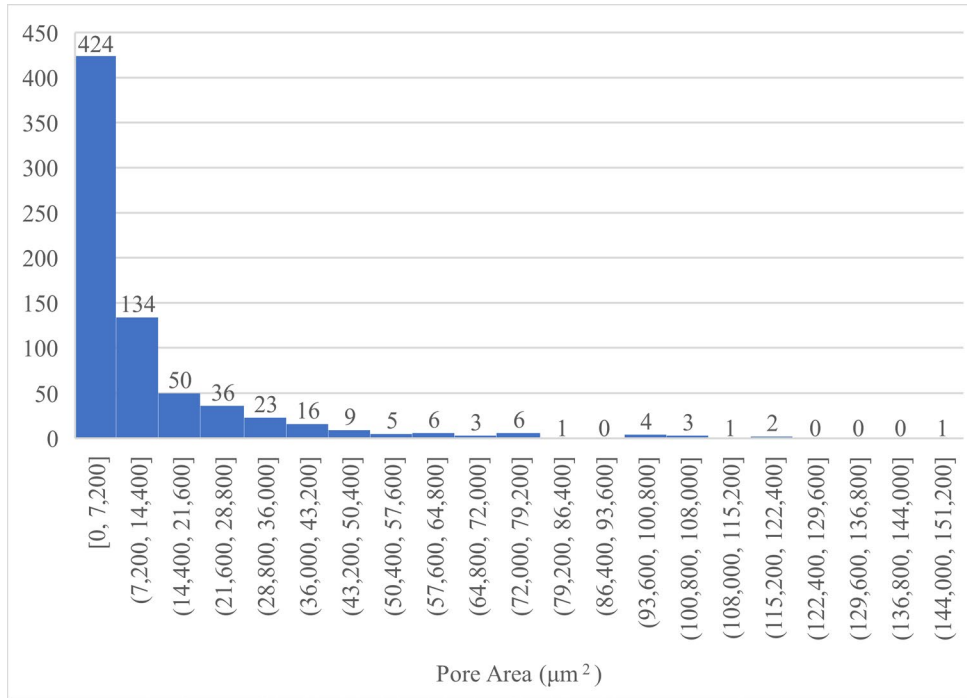


Figure 21. Pore area distribution of 3 wt% BNNB 0.5 wt% CNT

In the 3 wt% BNNB sample an area of  $26,721,895.6 \mu\text{m}^2$  was observed. In that area there was 703 pores. There was one outlier in the data in sample area 2 where one pore had an area of  $403,278.2 \mu\text{m}^2$ . This pore was omitted in the above histogram for better understanding of the size distribution of the remaining pores. The pores 60.31% of the porosity distribution occurring in the  $0 - 7,200 \mu\text{m}^2$  range. 19.06% of the porosity distribution occurring in the  $7,200 - 14,400 \mu\text{m}^2$  range. 7.11% of the porosity distribution occurring in the  $14,400 - 21,600 \mu\text{m}^2$  range. This data shows that majority of the pores were larger than those in both the 0 wt% and 1 wt% BNNB samples however fewer pores were present. As seen before, the increase of porosity drops in occurrence the larger the pore becomes. In the five sampled areas across the 3 wt% BNNB loading puck the percentage of the surface covered in pores ranged from 25.48% to 38.11%. The sample area with the largest porosity had the one large outlier pore. The average surface area porosity percentage was 33.04%. The 3wt% loading had the greatest porosity of all the various loadings. The standard deviation of the porosity area was  $23,602.612 \mu\text{m}^2$ .

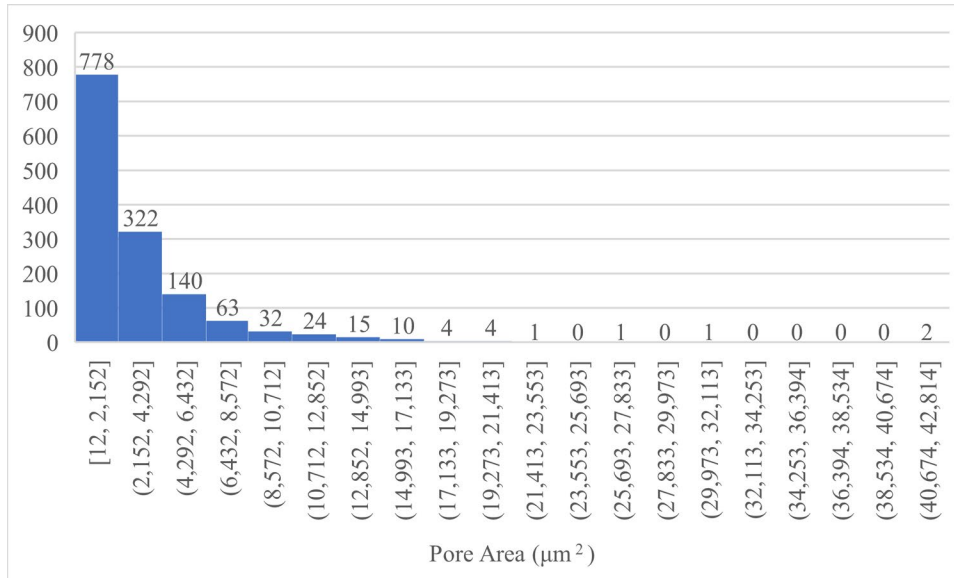


Figure 22. Pore area distribution of 5 wt% BNNB 0.5 wt% CNT

In the 5wt% BNNB sample an area of 25,789,121.5  $\mu\text{m}^2$  was observed. In that area there was 1,397 pores. The pores 55.69% of the porosity distribution occurring in the 12 – 2.152  $\mu\text{m}^2$  range. 23.05% of the porosity distribution occurring in the 2.152 – 4,292  $\mu\text{m}^2$  range. 10.02% of the porosity distribution occurring in the 4,292 – 6,432  $\mu\text{m}^2$  range. This data shows that majority of the pores were smaller than those in both the 3 wt% BNNB samples and however more pores were present. The pores were in general smaller than the pores found in the 1 wt% and the 0 wt% BNNB loadings. As the increase of porosity drops in occurrence the larger the pore becomes. In the five sampled areas across the 5 wt% BNNB loading puck the percentage of the surface covered in pores ranged from 14.17% to 18.61%. The average surface area porosity percentage was 16.08%. This sample had the least porosity of all the various loadings. The standard deviation of the porosity area was 3,733.31  $\mu\text{m}^2$

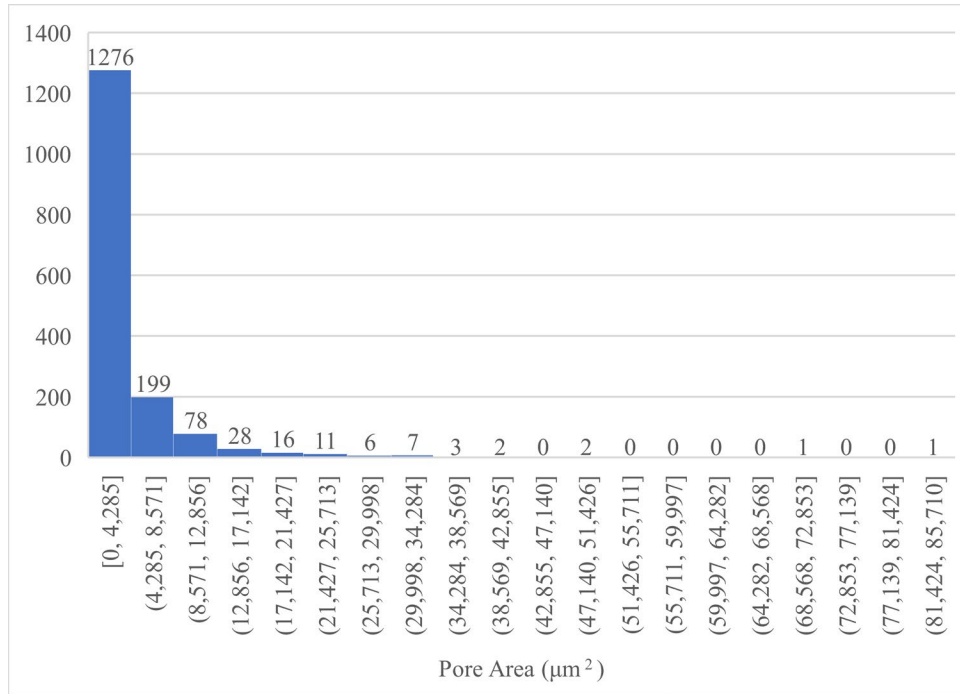


Figure 23. Pore area distribution of 10 wt% BNNB 0.5 wt% CNT

In the 10 wt% BNNB sample an area of 26,976,961  $\mu\text{m}^2$  was observed. In that area there was 1,630 pores. In sample area 3 there was one outlier pore with an area 497,501  $\mu\text{m}^2$ . The above histogram has removed that data point for better understanding of how most of the pores were distributed. For calculating the porosity percentages this large pore was included. 78.28% of the porosity distribution occurred in the 0 – 4,285  $\mu\text{m}^2$  range. 12.21% of the porosity distribution occurring in the 4,285 – 8,571  $\mu\text{m}^2$  range. 4.79% of the porosity distribution occurring in the 8,571 – 12,856  $\mu\text{m}^2$  range. In the five sampled areas across the 10 wt% BNNB loading puck the percentage of the surface covered in pores ranged from 17.02% to 23.11%. The average surface area porosity percentage was 19.44%. The standard deviation of the porosity area was 5,831.63  $\mu\text{m}^2$ .

### 3. SEM Imagery

Scanning electron microscopy has been used to study the morphology and surface imaging of various materials. Samples being studied in SEMs need to be electrically conductive for an image to be successfully produced. The electron beam interacts with the surface and reflects off the conductive surface to create a topographical image of the

surface of a specimen. If the sample is not organically conductive then a thin coating of electrically conductive material like gold is sputtered onto its surface. As previously mentioned in the introduction, CNT preforms like a metallic structure whereas BNNT preforms as a semiconductor. Since CNT preforms like a semimetal, it can be expected to be observed by the SEM without adding an additional coating. In order to identify where CNT is deposited in a nonconductive filler material, this method of imagine a raw specimen used. However, can BNNB's be seen in the same respect? It will be reasonable to think that they can since BNNTs have semiconducting properties, the barb version of boron nitride may be similar in that respect. If the BNNB also preforms like a semiconductor, the SEM will be able to successfully image these particles as well.

SEM imaging was conducted on polished cured BNNB-CNT composite samples at the 1 and 5 wt% BNNB loadings. In imaging the various loadings of BNNB, the objective was to be able to determine if agglomeration of BNNB exists at higher loadings. This agglomeration could explain the decrease in electrical conductivity and explain how the thermal conductivity improves with increased BNNB.

In Figure 24. 1 wt% BNNB we see in cured and polished epoxy pucks via InLens electron imaging. The network is a well dispersed network of CNT-BNNB particles. The image generated shows various depths at which particles are detected. The brighter the image the closer the particles are to the surface. At 5 wt% BNNB loading we can see a wider dispersion of the particles throughout the observable field. There is greater brightness in the 5 wt% BNNB loading may be due to the increased presence of boron nitride in the composite. If this is the case, then it is reasonable that the BNNB also behaves like a semiconductor like its BNNT counterpart.



Figure 24. Top: 1 wt% BNNB 0.5 wt% CNT SEM image 3000x, Bottom: 5 wt% BNNB 0.5 wt% CNT SEM image 3000x

As shown in Figure 25 at greater magnifications the interspersed depths of the CNT-BNNB particles become more apparent. At this loading of 5 wt% you can see that the CNT-BNNB particles tends to agglomerate into sections throughout the epoxy mixture. The SEM image's brighter sections are interpreted as sections closer to the surface of the

epoxy system whereas the grey tones are representative of structures deeper under the epoxy surface. The ImageJ generated surface plots of the BNNB-CNT networks are attempting to represent the tridimensional nature of the networks based on the grey tones found in the SEM images. In other studies of the percolation thresholds of CNT have found that at very low levels of CNT, below 0.1 wt%, there is not robust enough CNT networks to enable electrons to hop from nanotube to nanotube [22]. Similarly, when comparing our resistivity results when adding more BNNB the CNT networks become enveloped in the BNNB structures. The electrons are less able to hop from CNT to CNT, thus there is a decreased electrical performance of the CNT networks.

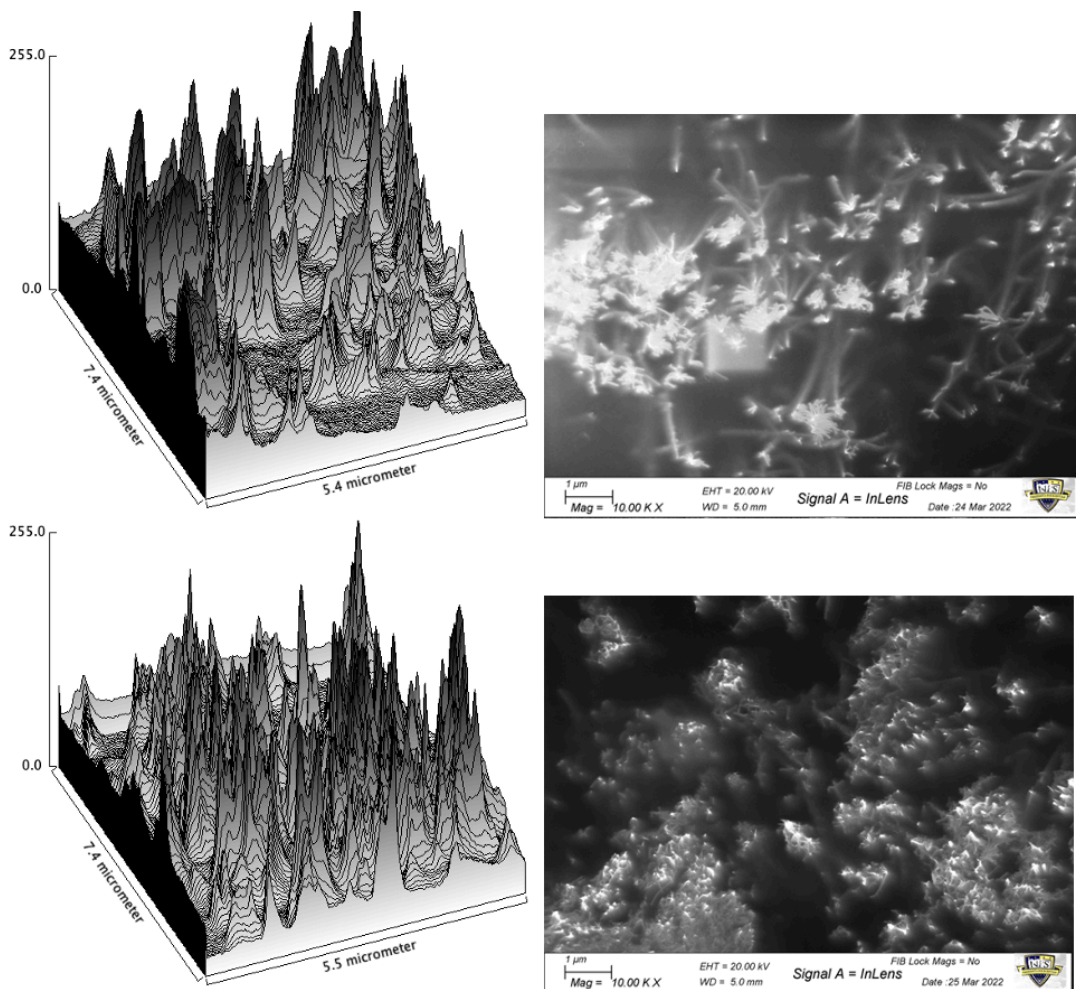


Figure 25. Top: 1 wt% BNNB 0.5 wt% CNT composite Bottom: 5 wt% BNNB 0.5 wt% CNT composite SEM image 10,000x

Literature has successfully imaged BNNT raw pulp at 20,000x with EHT of 15 kV [25]. In the 50,000x SEM image as shown in Figure 26 we see a webbing like structures the webbing indicating BNNB-CNT locations, although these webbed structures look different from the traditional tube-like structures that are normally found when imaging only CNT. The following EDS characterization section seeks to explain what is being observed in the bright webbed sections of the SEM image.

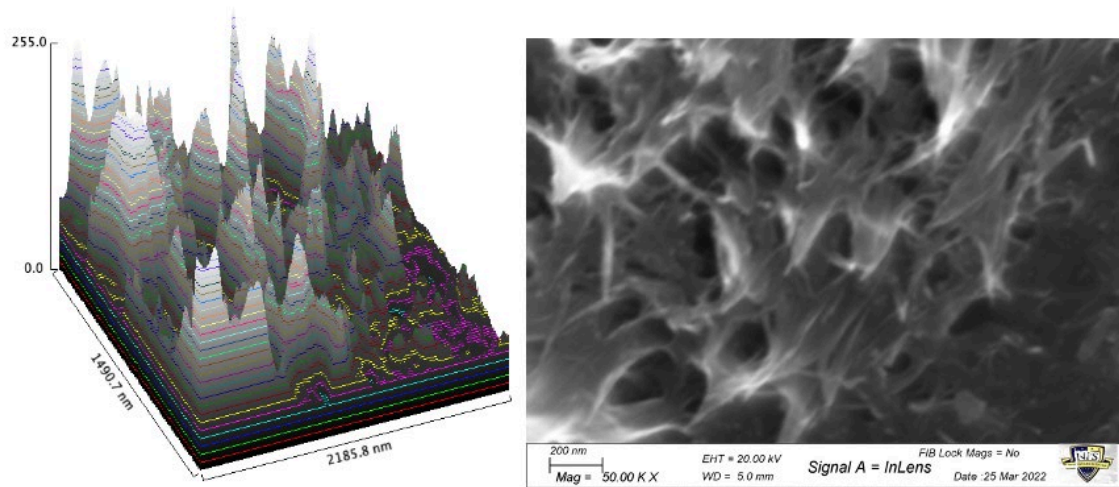


Figure 26. 5 wt% BNNB 0.5 wt% CNT SEM image 50,000x

#### 4. EDS Characterization

This section examines the results of energy dispersive spectroscopy of 5 wt% BNNB 0.5 wt% CNT in cured epoxy. The EDS results showed the chemical analysis of the sample. To image the CNT and BNNB we achieved an SEM image in the magnification range of 3000x. This will enable us to see broad swaths of CNT networks. Four spots were selected to compare the secondary electron ionization at these various locations.

Shown in Figure 27, EDS spot 1, spot 2 are in bright section of the SEM image. We had hypothesized that these sections showed where CNT were located. We were unsure of whether BNNB also gathered only at these locations. To decipher whether BNNB populated the bright sections and or the dark sections. EDS spot 3 was selected in a dark

location and EDS spot 4 was in a less bright section. As previously discussed, the brighter sections reflect CNT that was closer to the polished surface of the puck.

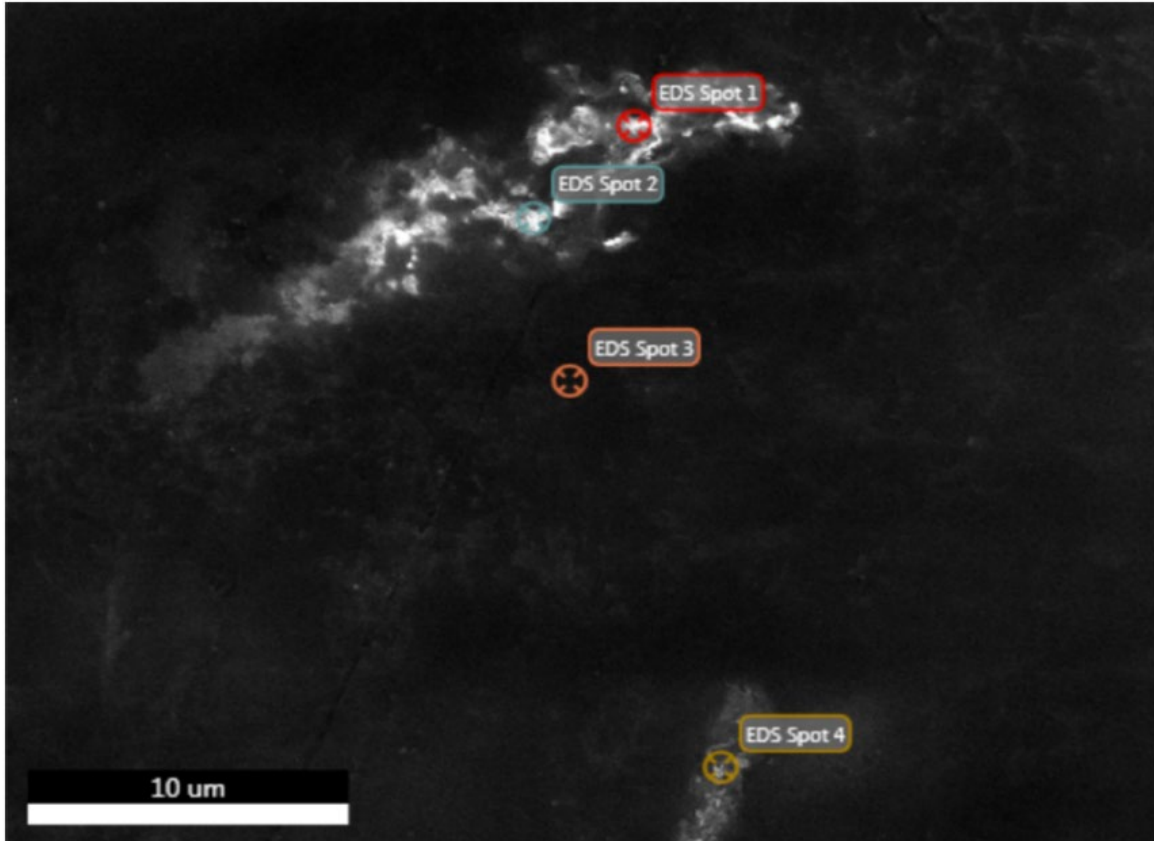


Figure 27. 5 wt% BNNB 0.5 wt% CNT SEM image 3000x used for EDS characterization. spot 1 (RED), spot 2 (TEAL), spot 3 (ORANGE), spot 4 (YELLOW)

Figure 28 shows the EDS spectra count for spots 1 and 2 in bright locations in the SEM image.

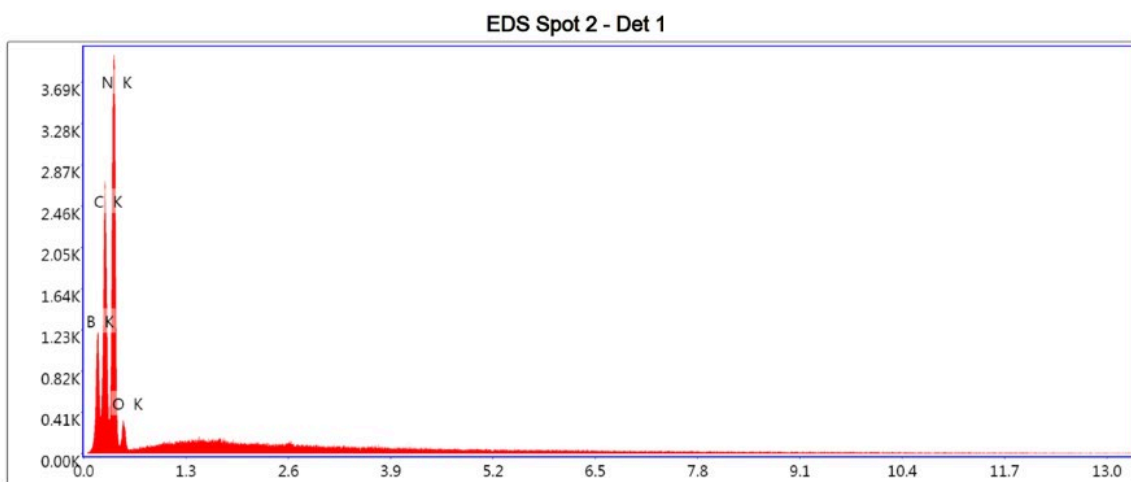
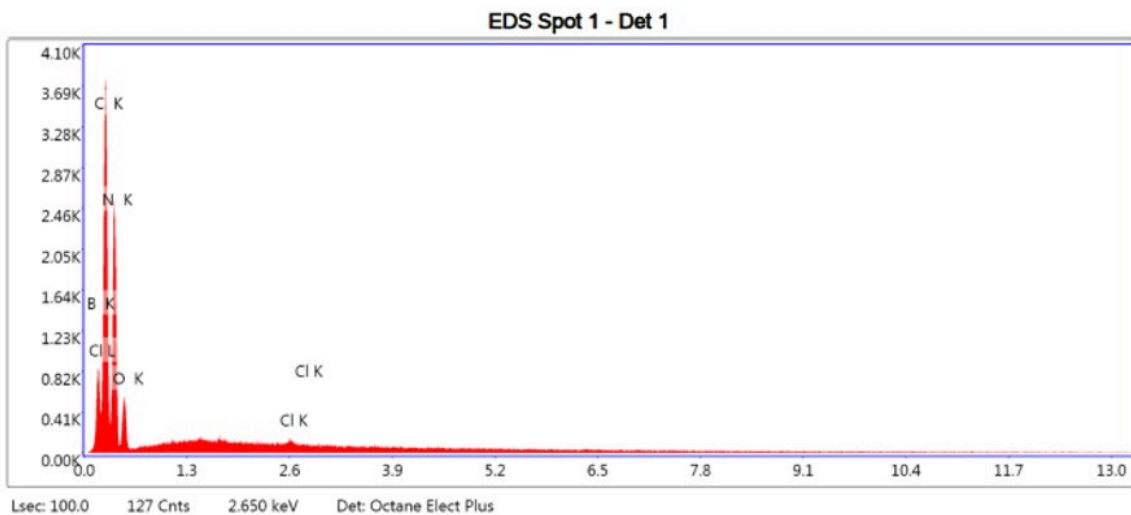


Figure 28. 5 wt% BNNB 0.5 wt% CNT EDS results spot 1 (top) and spot 2 (bottom)

At EDS spots 1 and 2 we see several energy spikes at a bright section of the SEM image. These spikes correlate to the K energy band to various elements in the sample. The energy spikes at spot 1 correlate to Boron, Carbon, Nitrogen, Oxygen and Chlorine. The energy spikes at spot 2 correlate to Boron, Carbon, Nitrogen and Oxygen. Chlorine is most likely contaminant and was dismissed in the results.

Table 2. 5 wt% BNNB 0.5 wt% CNT EDS quantitative results spot 1 (top) and spot 2 (bottom)

**eZAF Smart Quant Results**

Element	Weight %	Atomic %	Net Int.	Error %	Kratio	Z	A	F
B K	15.78	18.59	82.22	7.94	0.0683	0.9719	0.4455	1.0000
C K	37.24	39.49	418.20	9.00	0.0953	1.0204	0.2508	1.0000
N K	40.34	36.68	273.13	10.67	0.0453	0.9958	0.1128	1.0000
O K	6.54	5.20	55.69	13.31	0.0058	0.9745	0.0906	1.0000
Cl K	0.11	0.04	9.13	26.35	0.0009	0.8219	1.0278	1.0228

**eZAF Smart Quant Results**

Element	Weight %	Atomic %	Net Int.	Error %	Kratio	Z	A	F
B K	20.57	24.17	124.29	7.56	0.0902	0.9746	0.4499	1.0000
C K	27.43	29.02	291.73	9.59	0.0581	1.0232	0.2070	1.0000
N K	48.70	44.18	440.33	10.22	0.0638	0.9985	0.1312	1.0000
O K	3.31	2.63	30.84	15.34	0.0028	0.9771	0.0863	1.0000

The challenge to detect Boron and Carbon relates to the limitations of the EDS detector. EDS is limited in detecting lighter elements like Boron because it has lower characteristic K energy level shell compared to heavier elements' characteristic K energy level shell Xray which is easier to detect. The Xray count detected at this section of the SEM image for Boron is most likely relatively low artificially due to Boron being at the limits of the EDS detection capabilities. BNNB is made of equal parts Boron and Nitrogen. For that reason, the Nitrogen spike may have a better representation of the BNNB in the sample since the K energy level of Nitrogen is easier to detect. The Carbon spike should be representative of the CNT in the sample.

Figure 29 shows the EDS spectra count for spot 3, a dark location in the SEM image.

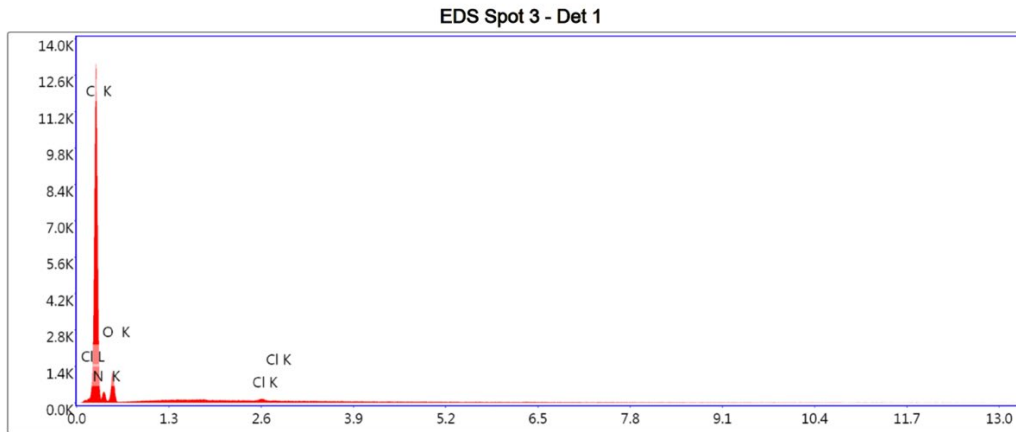


Figure 29. 5 wt% BNNB 0.5 wt% CNT EDS results spot 3

At EDS spot 3 we observe energy spikes at a dark location of the SEM image. The energy spikes at spot 3 correlate to Carbon, Nitrogen, Oxygen and a small Chlorine spike. There is notably less nitrogen and no boron observed at this location. The BNNB maybe clumping around CNT and that is why the Nitrogen is detected greater in those regions versus in the darker locations.

Table 3. 5 wt% BNNB 0.5 wt% CNT EDS quantitative results spot 3

**eZAF Smart Quant Results**

Element	Weight %	Atomic %	Net Int.	Error %	Kratio	Z	A	F
C K	68.77	73.55	1438.92	3.96	0.5032	1.0114	0.7234	1.0000
N K	13.19	12.10	40.20	14.64	0.0102	0.9870	0.0786	1.0000
O K	17.75	14.25	117.16	12.07	0.0186	0.9660	0.1086	1.0000
Cl K	0.29	0.10	16.00	16.93	0.0025	0.8148	1.0234	1.0213

From the quantitative results found in spot 3, there is a significant decrease in nitrogen when compared to spot 1 and 2. Spot 3 had 27.1% of the Nitrogen compared to spot 2. However, the error percent did increase from 10 to 14.64%. This may be due to there being less nitrogen to detect thus more uncertainty when detecting lower quantities of nitrogen.

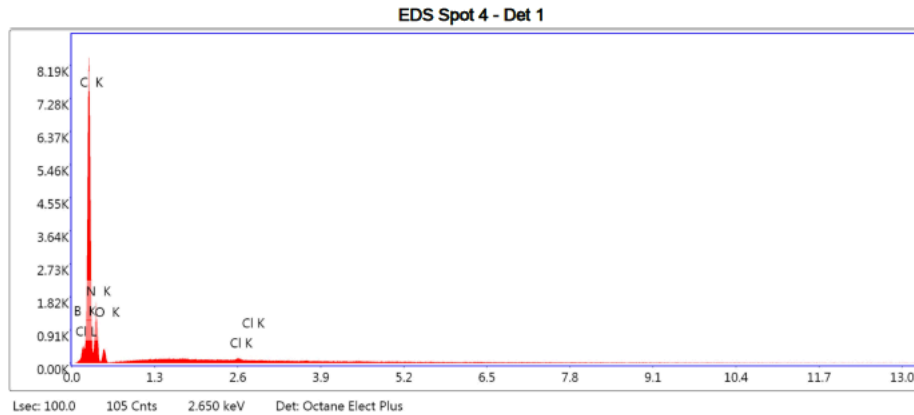


Figure 30. 5 wt% BNNB 0.5 wt% CNT EDS results spot 4

At EDS spot 4 we observe energy spikes at a medium grey location of the SEM image. The energy spikes at spot 4 correlate to Boron, Carbon, Nitrogen, Oxygen and Chlorine. There is notably more Nitrogen and some Boron observed at this location when compared to spot 3 where no Boron was detected. The BNNB maybe present at this location but at a lesser amount than at spots 1 and 2.

Table 4. 5 wt% BNNB 0.5 wt% CNT EDS quantitative results spot 4

**eZAF Smart Quant Results**

Element	Weight %	Atomic %	Net Int.	Error %	Kratio	Z	A	F
B K	8.28	9.69	43.98	8.58	0.0371	0.9659	0.4639	1.0000
C K	53.85	56.70	907.62	7.43	0.2102	1.0141	0.3849	1.0000
N K	33.20	29.98	178.23	11.14	0.0300	0.9897	0.0914	1.0000
O K	4.53	3.58	37.21	14.37	0.0039	0.9685	0.0892	1.0000
Cl K	0.13	0.05	11.32	21.22	0.0012	0.8168	1.0312	1.0233

From the quantitative results found in spot 4, there is a significant increase in nitrogen when compared to spot 3. Spot 4 had 252% more the Nitrogen compared to spot 3. The error percent decreased from 14.64% to 11.14%. As more nitrogen is observed the less uncertainty exists when detecting higher quantities of nitrogen.

THIS PAGE INTENTIONALLY LEFT BLANK

## IV. CONCLUSION

The objective of this thesis was to gain a sufficient understanding of the fabrication variables that affect the thermal conductive properties of the CNT composites and propose a model to explain the mechanism of conduction based on experimental observations. This objective was achieved through the fabrication, testing, and characterization of BNNB-CNT and epoxy-CNT composites produced with a variable range of boron nitride nanobarb loadings.

As a result, we saw an increase in thermal conductivity as BNNB loadings increased. Various factors like porosity and agglomeration of BNNB at higher loadings were observed. Porosity observed from the optical microscopy images was analyzed on imageJ and the distributions are found in Figure 31.

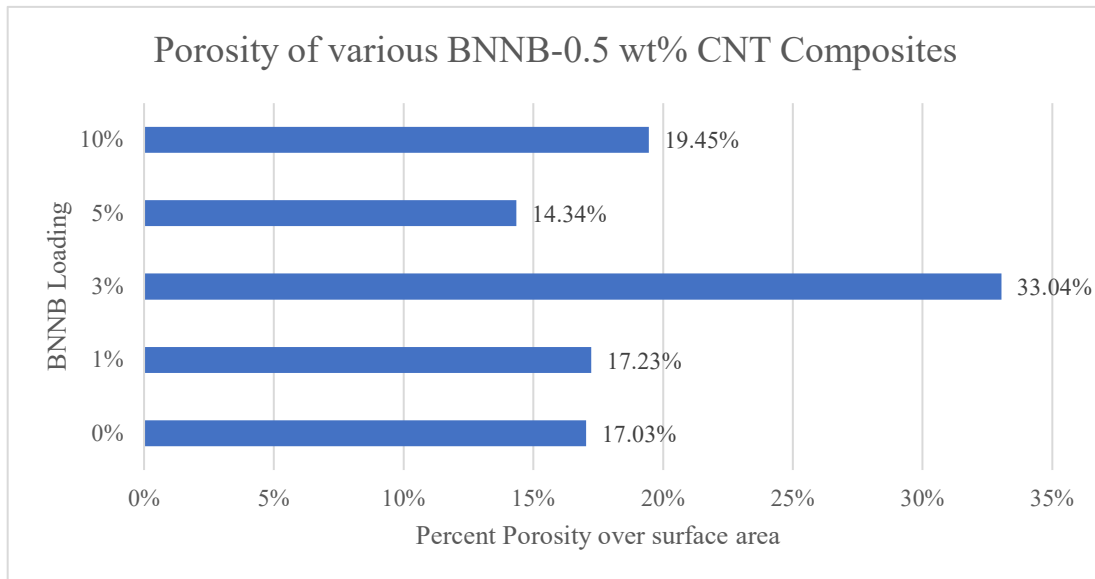


Figure 31. Porosity of various BNNB loadings

When normalizing the thermal conductivity data against the found porosity of each BNNB loading we take into consideration Equation 11:

$$\text{Equation 10. } K_s * A_s * (T_1 - T_2) / L_s = K_c * A_c * (T_2 - T_3) / L_c$$

Rearranging Equation 11 gives us the formula for Thermal Conductivity found in Equation 12.

$$\text{Equation 11. } K_c = [K_s * A_s * (T_2 - T_1) / L_s] / A_c * (T_2 - T_1) / L_c$$

To better understand the role porosity plays in the resulting thermal conductivity, we alter Equation 10 to account for this porosity factor. To do this the surface area of the composite,  $A_c$ , is multiplied by (1-porosity%) exclude the average porosity area from its cross-sectional area. As elements of the original equation cancel out due to previously discussed assumptions, it results in the previously found  $K_c$  being divided by the percent of the area that does not have pores. From the previous assumption that the contact area between the steel block and the composite are the same, we can cancel out the areas to get the following equations.

$$\text{Equation 12. } K_c = [K_s * (T_1 - T_2) / L_s] / [(1 - \text{porosity}) * (T_2 - T_3) / L_c]$$

$$\text{Equation 13. } K_c = [K_s * (T_1 - T_2) * L_c] / [(1 - \text{porosity}) * (T_2 - T_3) * L_s]$$

However, this assumption was false. Upon closer inspection of the BNNB-CNT composite samples found some variation in the composite surface area. To account for this the area component was measured for each sample and then, the thermal conductivity was calculated using the associated area terms.

$$\text{Equation 14. } K_c = [K_s * A_s * (T_1 - T_2) * L_c] / [(1 - \text{porosity}) * A_c * (T_2 - T_3) * L_s]$$

It was found that area variations did have a significant effect on the resulting thermal conductivity of the BNNB-CNT composite samples. The resulting error is documented in Table 3.

Table 5. Thermal Conductivity error caused by composite cross-sectional area deviations

Various BNNB Loadings of 0.5wt% CNT Epoxy Composites	Percent Error Caused by Area deviations between Steel Block and Composite
0%	4.03
1%	13.85
3%	1.51
5%	17.08
10%	7.13

The greatest inconsistencies in composite area were found in the 1wt% BNNB loading and 5wt% BNNB loading. The cut off machine used in this study suffered from a blade alignment issue which complicated achieving high accuracy cuts. A more accurately aligned blade would have reduced this error.

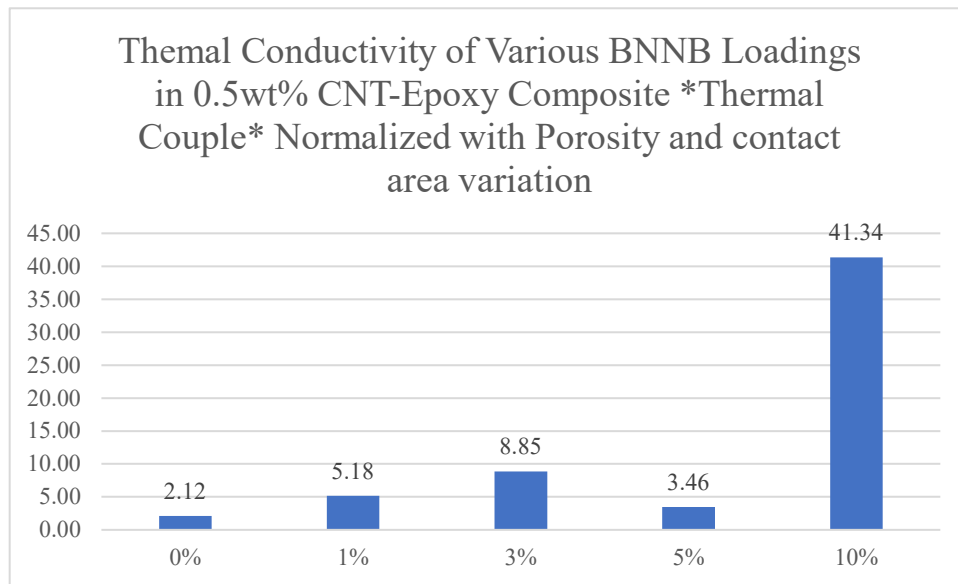


Figure 32. Resulting Thermal Conductivity data from thermal couple data collection design that has been normalized with area variation and porosity

This data show that when adding 1wt% BNNB to the 0.5wt% CNT-Epoxy composite that the thermal conductivity improved by 244.71% when compared to the 0.5

wt% CNT-Epoxy mixture sans BNNB. When adding 3 wt% BNNB to the 0.5 wt% CNT-Epoxy composite the thermal conductivity improved by 418%. When adding 5 wt% BNNB to the 0.5 wt% CNT-Epoxy composite the thermal conductivity improved by 163% compared to the no BNNB baseline composite. When adding 10 wt% BNNB to the 0.5 wt% CNT-Epoxy composite the thermal conductivity improved by 1953%.

Thorough investigation as to why the 5 wt% percentage BNNB loading did not result in a more significant increase in thermal conductivity remains unclear. After scrupulous comparison of the thermal conductivity studies revealed the frame rate for the 5 wt% percent thermal couple thermal conductivity data gathering was found at 12 frames a minute versus 60 frames a minute in the other studies. Future studies would have to compare whether agglomeration of the 5 wt% BNNB composite occurred in a way that prevented equitable dispersion of the BNNB throughout the composite.

The EDS data gathered concluded that BNNB agglomerated around CNT locations. So that informs all the SEM images locations of the BNNB are collocated at the bright CNT locations.

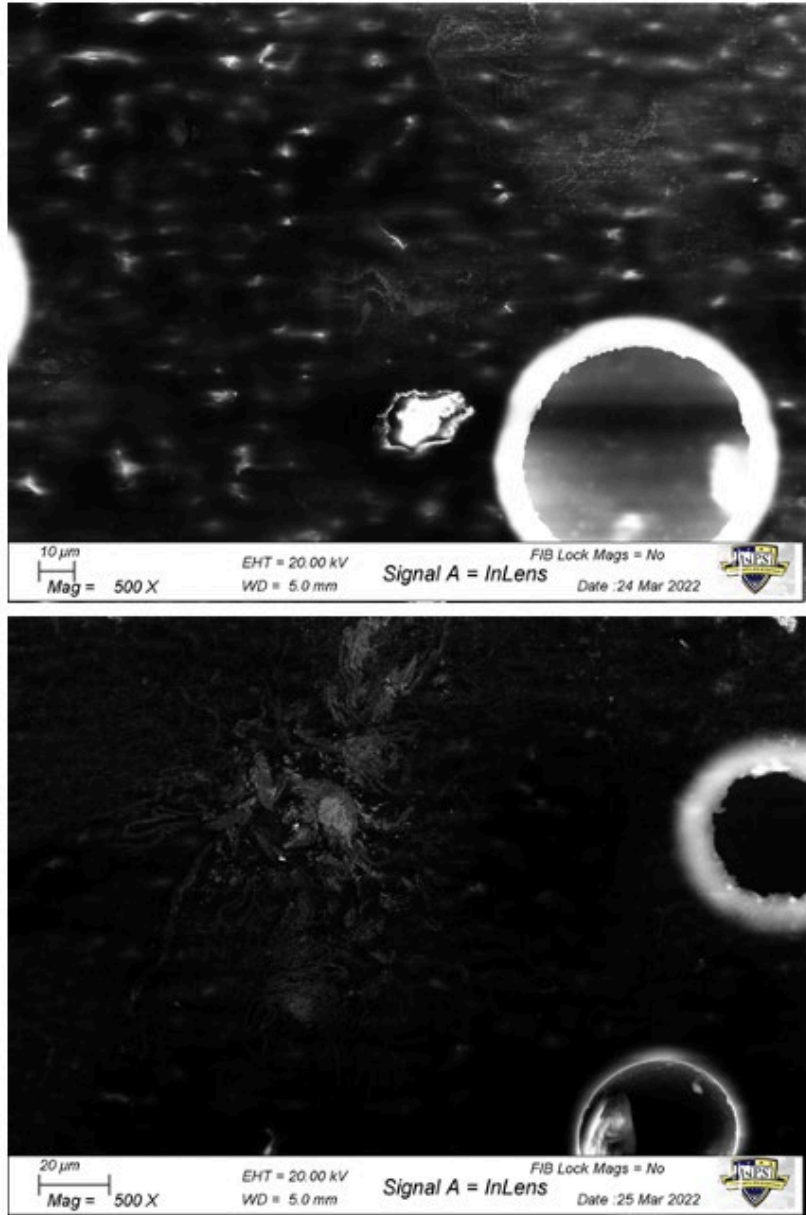


Figure 33. Top: 1% BNNB, Bottom 5% BNNB loading

From comparing two 500X SEM images of the 1 wt% and 5 wt% BNNB loadings, the BNNB and CNT are agglomerated at a few locations in the 5wt% sample versus spaced through the field of view evenly in the 1 wt% sample. The agglomeration of BNNB unevenly through the sample could be why there is a lower-than-expected thermal conductivity found in this study. Poor dispersion allows for less heat to be dissipated through the composite.

THIS PAGE INTENTIONALLY LEFT BLANK

## V. DISCUSSION AND RECOMMENDATIONS

This section discusses what future studies of BNNB composites could help further our understanding of how they affect CNT composites as thermal conductivity additive. Thus far in our research preliminary batches of BNNB-CNT composites have been made at 1, 3, 5 and 10 wt% BNNB loadings in a 0.5 wt% CNT epoxy composite. These loadings were tested to find their associated electrical resistivities and a relative idea as to how their thermal conductive properties behave.

### A. FUTURE STUDIES

Future studies should examine higher BNNB loadings such as 15, 20 and 25 weight percentages to determine if the trend for thermal conductivity normalized with porosity continues in a linear relationship or if it shifts to an exponential relationship.

It will be beneficial to conduct an agglomeration study of all BNNB loadings with SEM and EDS to better understand the dispersion of BNNB at each loading with higher fidelity. By taking EDS analysis at each loading will reinforce the conclusion that BNNB gathers at CNT network sites.

Study how thickness impacts thermal conductivity, how thin can we make these components to have the same thermal conductivity.

Not included in this study was the repeated 5 wt% BNNB study. Both the original and repeated 5wt% BNNB loading CNT-composite had unexpectedly low thermal conductivity values. Another future study could delve further into repeating synthesis and repeating loadings to see if this trend at 5 wt% BNNB loading continues and what possible explanation could be occurring.

The magnitude of thermal conductivity is affected by aspects such as thickness and temperature. Wiedemann-Franz law describes the effect temperature has on thermal conductivity. When there is a temperature increase in a sample the internal velocity transfers heat more efficiently and thus thermal conductivity increases [16]. It is important to note that the relationship between temperature and thermal conductivity is nonlinear.

For this study the hotplate was heated to a desired 50°C. There were fluctuations in what the set temperature heated to due to the imprecise nature of the hotplate. Most temperatures ranged from 45°-55°C. Since all temperatures were in the same order of magnitude it was assumed that the effects of temperature were negligible. Future studies could include examining these BNNB loadings at higher temperatures to better understand how high heat affects the BNNB-CNT composite thermal conductivity.

## **B. PROCESS IMPROVEMENTS**

This section discusses general recommendations for future synthesis of BNNB-CNT epoxy pucks for improved quality and design consistency. One process improvement would be to create them thinner and place them under a higher vacuum for a period before placing them in the furnace to cure. Creating a thinner puck should prevent thermal run away causing a foaming porous effect throughout the sample. Also placing the samples under a higher vacuum could help remove any remaining bubbles in the epoxy generated in the mixing process.

It would be useful to compare the results of other thermal conductivity collection methods where all surfaces of the experiment are insulated to be able to determine the error from concessions made for FLIR data collection such as having a wall exposed for observation. This would indicate how the FLIR set up potentially impacts the repeatability/accuracy of the resulting data collected.

Omega RDXL6SD Six Channel Handheld Temperature Data Logger temperature accuracy  $\pm 0.1\%$  or  $0.8^\circ\text{C}$  for temperatures below  $1000^\circ\text{C}$  [26].

FLIR ETS320 accuracy  $\pm 3^\circ\text{C}$  or  $\pm 3\%$  of reading for ambient temperature  $10^\circ\text{C}$  to  $35^\circ\text{C}$ , Important to note that the experiment was conducted at  $50^\circ\text{C}$  outside of these parameters outlined on the FLIR technical data sheet [27].

## LIST OF REFERENCES

- [1] MaxwellMolecule, "Thermal Conductivity," 19 January 2029. [Online]. Available: [https://en.wikipedia.org/wiki/File:Simple\\_definition\\_of\\_thermal\\_conductivity.png](https://en.wikipedia.org/wiki/File:Simple_definition_of_thermal_conductivity.png). [Accessed 7 August 2022].
- [2] H. e. A. Pang, "Conductive Polymer Composites with Segregated Structures," *Progress in Polymer Science*, vol. 39, no. 11, p. 908–1933, 2014.
- [3] S. J. P. D. G. S. V. J. M. a. C. L. B. Earp, "Electrically Conductive CNT Composites at Loadings below Theoretical Percolation Values," *Nanomaterials*, vol. 9, no. 4, p. 491, 2019.
- [4] K. M. A. E.-N. R. A. A. A. A.-W. Ahmad Aqel, "Carbon nanotubes, science and technology part (I) structure, synthesis and characterisation," *Arabian Journal of Chemistry*, vol. 5, pp. 1–23, 2012.
- [5] T. S. B. R. H. A. De Volder, "Carbon Nanotubes: Present and Future Commercial Applications," *Science*, vol. 339, pp. 535–539, 2013.
- [6] D. S. M. Junjie Wu, "Scaling behavior of the complex conductivity of graphite-boron nitride percolation systems," *Physical Review*, vol. 58, no. 22, 1998.
- [7] D. J. Bogumiła Kumanek, "Thermal conductivity of carbon nanotube networks: a review," *J Mater Sci*, vol. 54, pp. 7397–7427, 2019.
- [8] T. V. P. J. H. H. C. S. K. a. M. J. K. Jun Hee Kim, "Boron nitride nanotubes: synthesis and applications," *Nano Convergence*, vol. 5, no. 17, pp. 1–23, 2018.
- [9] BNNano, "Transforming and Revitalizing Industrial Commodities," BNNano Inc, 2022. [Online]. Available: <https://www.bnnano.com/>. [Accessed 7 August 2022].
- [10] S. McDonald, "Team Discovers New Method of Making Promising Material," NASA, 31 August 2017. [Online]. Available: <https://www.nasa.gov/feature/langley/team-discovers-new-method-of-making-promising-material>.
- [11] Loctite, "LOCTITE EA 9396 AERO Technical Process Bulletin," Henkel Cooperation Aerospace, Bay Point CA, 2013.

- [12] Ellsworth Adhesives, “HENKEL LOCTITE EA 9396 AERO EPOXY ADHESIVE 1 QT KIT,” Ellsworth Adhesives, 2022. [Online]. Available: <https://www.ellsworth.com/products/adhesives/epoxy/henkel-loctite-hysol-ea-9396-epoxy-adhesive-1-qt-kit/>. [Accessed 7 August 2022].
- [13] Huntsman International LLC, “MIRALON,” HUNTSMAN, 2022. [Online]. Available: <https://www.huntsman.com/products/detail/344/miralon/dispersed-products>. [Accessed 7 August 2022].
- [14] Huntsman International LLC, “MIRALON Products Technical Datasheet,” Huntsman Corporation, The Woodlands, TX, 2020.
- [15] Keithley, “Resistivity Measurements of Semiconductor Materials Using the 4200A-SCS Parameter Analyzer and a Four-Point Collinear Probe,” Tektronix, 2016.
- [16] Akoss, “Understanding Thermal Conductivity,” QATS Advanced Thermal Solutions Inc., 21 October 2011. [Online]. Available: <https://www.qats.com/cms/2011/10/21/understanding-thermal-conductivity/>.
- [17] Arctic Silver, Inc., “Arctic Silver 5 High-Density Polysynthetic Silver Thermal Compound,” Arctic Silver, Inc., 2022. [Online]. Available: <https://www.arcticsilver.com/as5.htm>. [Accessed 7 August 2022].
- [18] ATSM International, “Standard Test Method for Thermal Conductivity of Solids by Means of the Guarded Comparative-Longitudinal Heat Flow Technique,” *ATSM International*, vol. 1225, no. 04, 13 January 2016.
- [19] Teledyne FLIR LLC, “FLIR ETS320,” 2022. [Online]. Available: <https://www.flir.com/products/ets320/?vertical=rd+science&segment=solutions>.
- [20] SAMWOO, “Epiphot 200 for Brightfield and Darkfield Observations,” SAMWOO, [Online]. Available: <http://samwoosc.co.kr/Nikon/epiphoto200.htm>. [Accessed 7 August 2022].
- [21] ZEISS, “ZEISS Sigma Field Emission Scanning Electron Microscope,” [Online]. Available: <https://www.zeiss.com/microscopy/int/products/scanning-electron-microscopes/sigma.html>. [Accessed 7 August 2022].
- [22] J. P. D. G. S. V. M. P. C. L. B. Earp, “Impact of current and temperature on extremely low loading epoxy-CNT conductive composites,” *Polymers*, vol. 4, no. 867, 12.

- [23] M. Mau, "LOCTITE EA 9396C-2 AERO PART A Safety Data Sheet," Henkel, 2014.
- [24] West System, "The Basics of Uncontrolled Cure," Epoxy Works, 2022. [Online]. Available: [HTTPS://WWW.WESTSYSTEM.COM/SAFETY/UNCONTROLLED-CURE/](https://www.westsystem.com/safety/uncontrolled-cure/).
- [25] RAYMOR Nanotubes for Electronics, "Boron Nitride Nanotubes - BNNT multi-walled powder," Raymor Industries Inc., 2022. [Online]. Available: <https://raymor.com/our-products/boron-nitride-nanotubes-bnnt/>. [Accessed 9 August 2022].
- [26] OMEGA, "Six Channel Handheld Rechargeable Temperature Data Logger," Omega Engineering, Inc, 2022. [Online]. Available: <https://www.omega.com/en-us/temperature-measurement/temperature-and-humidity-data-loggers/p/RDXL6SD-USB-Series>.
- [27] FLIR Systems Inc., "FLIR ETS320 Datasheet," 2017. [Online]. Available: [www.flir.com/science](http://www.flir.com/science).
- [28] S. A. a. A. Z. Masa Ishigami, "Properties of Boron Nitride Nanotubes," *AIP Conference Proceedings*, vol. 94, p. 696, 2003.

THIS PAGE INTENTIONALLY LEFT BLANK

## INITIAL DISTRIBUTION LIST

1. Defense Technical Information Center  
Ft. Belvoir, Virginia
2. Dudley Knox Library  
Naval Postgraduate School  
Monterey, California